

**Organic semiconductors containing  
multi-heteroatom rings**

A thesis

presented to the

Department of Chemistry

of

Lakehead University

by

Clifford Agyei

in partial fulfillment of requirements for the degree of

Master of Chemistry

January 16<sup>th</sup>, 2018

## Abstract

Oligomers of thiophene are ubiquitous in molecular materials research. Other ring systems, especially those lacking at least  $C_{2v}$  symmetry are much less common. We investigated thiophene-thiazole, pyrrole-thiazole, thiophene-furan, and thiophene-selenophene co-oligomers, which nominally have the same conjugation length and physical dimensions as thiophene oligomers but contain a heteroatom, that should impact the electronic properties. The lower symmetry of the 1,3-thiazole system, among other attributes, makes these new systems chemically challenging to synthesize; however, the electronic and steric variability makes them interesting targets. One common method of synthesizing thiazole is the ring-closing reaction that generates an amino-substituted thiazole. We have done a systematic study to convert the aminothiazole to a more useful synthon using Sandmeyer conditions. We herein present the synthesis, characterization, and molecular or photoelectronic structures of selected mixed oligomer systems, along with a computational study to measure bond length alternation, localization indices, and HOMO-LUMO (band gap) energy. Aminothiazole can be deaminated using Sandmeyer conditions. As conjugation length increases with the addition of a more electron withdrawing group, there is a general decrease of the band gap as well as of the HOMO-LUMO energies

## Acknowledgement

I would like to thank almighty God for his guidance and protection throughout these years. I would like to express my sincere gratitude to my supervisor Dr. Craig Mackinnon for teaching me to be a synthetic chemist and allowing me to call the Mackinnon Lab home for the last two years. I would like to thank my committee members Dr. Robert Mawhinney, Dr. Stephen Kinrade, and Dr. Kai Ylijoki for their input and guidance in my research and the writing of this thesis.

I would like to thank Dr. Gregory Spivak of blessed memory and Dr. Christine Gottardo for their guidance, comments and input during this work.

I would like to thank the Lakehead University Chemistry technician team, Debbie Puumala, Brad Miller, Christina Richards, and Jarrett Sylvestre for fixing everything I broke and answering all my questions.

I would like to extend many thanks to Dr. Michael Campbell for running our samples on the mass spectrometer.

Lastly to my lovely wife, Philippa, my daughters; Alexandra, Maame Yaa, Akosua and Pamela for their support throughout the years.

# Table of Contents

Abstracts.....	i
Acknowledgement .....	ii
Table of contents.....	iii
List of abbreviations .....	v
List of schemes .....	viii
List of figures.....	ix
List of tables .....	x
Chapter 1-Introduction.....	1
1.1 Semiconductivity.....	1
1.2 Introduction to molecular semiconductors.....	3
1.2.1 Current strategies for the production of semiconductors.....	4
1.2.2 Application of semiconductors.....	5
1.2.2.1 Organic photovoltaic cells.....	6
1.2.2.2. Organic light-emitting diodes (OLEDs) .....	8
1.2.2.3 Organic field-effect transistors (OFETs) .....	9
1.3 Hetero(aromatic) compounds .....	11
1.3.1 Heteroatoms.....	13
1.3.2 Chalcogenophenes.....	13
1.3.2.1 Oligothiophenes.....	13
1.3.2.2 Oligoselonophene .....	15
1.3.2.3 Oligofuran .....	15
1.3.2.4 Thiazole.....	16
1.4 Computational studies .....	16
1.5 Scope of thesis.....	16
Chapter 2-Sandmeyer reactions with heterocycles.....	20
2.1 Introduction.....	20
2.1.1 The Sandmeyer reaction.....	20
2.1.2 The Hantzsch thiazole synthesis.....	22
2.2 Results and discussion .....	23

2.2.1 Synthesis of 2-amino-4-hexyl-1,3-thiazole ( <b>1</b> ).....	23
2.2.2 Comparative analysis of Sandmeyer reactions.....	25
2.2.3 Synthesis of 2-bromo-4-hexyl-1,3-thiazole ( <b>2</b> ).....	27
2.2.4 Synthesis of 2,2'-diamino-4,4'-bithiazole.....	28
2.3 Experimental .....	29
2.3.1 General.....	29
2.3.2 Preparation of 2-amino-4-hexyl-1,3-thiazole.....	29
2.3.3 Preparation of 2-bromo-4-hexyl-1,3-thiazole.....	30
2.3.4 Synthesis of 2,2'-dibromo-4,4'-bithiazole.....	30
Chapter 3-Synthesis of mixed oligomers .....	31
3.1 Ring systems used in this study.....	32
3.2 Coupling methods.....	34
3.2.1 Grignard-type synthesis of oligomers.....	34
3.2.2 Synthesis of 2,2'-bis( <i>N</i> -pyrrolyl)-4,4'-bithiazole ( <b>12</b> ).....	37
3.2.3 Attempted synthesis of 5-(4-hexyl-1,3-thiazolyl)-2,2':5,2'-terthiophene ( <b>13</b> ).....	37
3.2.4 Attempted synthesis by Stille coupling of 5-(2-furanyl)-2,2':5,2''-terthiophene ( <b>14</b> )...38	
3.2.5 Suzuki coupling of 5-(2-furanyl)-2,2':5,2''-terthiophene ( <b>14</b> ).....	38
3.3 Results and discussion .....	39
3.4. Experimental .....	42
3.4.1 General synthetic and instrumental details.....	42
3.4.2 Preparation of 5,5'-bis(4-hexyl-2-methyl)-thiazolyl)-2,2'-bithiophene ( <b>9</b> ).....	43
3.4.2.1 Preparation of 4-hexyl-2-methyl-1,3-thiazole ( <b>4</b> ).....	43
3.4.2.2 preparation of 5-bromo-4-hexyl-2-methyl-1,3-thiazole ( <b>5</b> ).....	43
3.4.2.3 Preparation of 5,5'-bis(4-hexyl-2-methyl)-thiazolyl)-2,2'-bithiophene ( <b>9</b> ).....	44
3.4.3 Preparation of 5,5'-bis(2-furanyl)-2,2'-bithiophene ( <b>11</b> ).....	44
3.4.4 Preparation of 2,2'-bis( <i>N</i> -pyrrolyl)-4,4'-bithiazole ( <b>12</b> ).....	45
3.4.5 Suzuki coupling of 5-(2-furanyl)-2,2':5,2''-terthiophene ( <b>7</b> ).....	46
Chapter 4-Computational studies .....	47
4.0 Introduction .....	47
4.1. Monomers .....	50
4.1.1 HOMO-LUMO energies/band gap.....	51

4.1.2 Bond length alternation.....	52
4.1.3 Localization index.....	52
4.2 Dimers.....	53
4.2.1 HOMO-LUMO energies/band gap.....	56
4.2.2 Delocalization.....	59
4.3 Tetramers. ....	65
4.3.1 HOMO-LUMO energies/band gap.....	65
4.3.2 Delocalization.....	66
4.4 Conclusion .....	71
Chapter 5-Conclusion and future work.....	72
5.1 Conclusion .....	72
5.2 Future work.....	73
References.....	75
Appendix.....	82
Appendix 1.1 Attempted synthesis of 2,2'-bis(2-thienyl)-4,4'-bithiazole ( <b>8</b> ).....	82
Appendix 1.2 Attempted synthesis of 5,5'-bis (2-(4-hexyl)-thiazolyl)-2,2'-bithiophene ( <b>10</b> ).....	83
Appendix 1.3 Attempted synthesis 5-(4-hexyl-1,3-thiazolyl)-2,2':5',2''-terthiophene ( <b>13</b> ).....	84
Appendix 1.4 Attempted synthesis of 5-(2-furanyl)-2,2':4,2''-terthiophene via Stille coupling ( <b>14</b> ).....	84

## List of Abbreviations

amu	atomic mass unit
BLA	bond length alternation
C <sub>60</sub>	buckminsterfullerene
d	doublet (NMR descriptor)
D	length of nominally double bond
DMF	<i>N,N</i> -dimethylformamide
E <sub>g</sub>	energy gap
E <sub>H-L</sub>	HOMO-LUMO gap
eV	electronvolt
Fu	furan
HOMO	highest occupied molecular orbitals
Hx	hexyl group
Hz	hertz
J	NMR coupling constant
LI	localization index
LUMO	lowest unoccupied molecular orbitals
M	molarity
m/z	mass to charge ratio
mmol	millimole
NBS	<i>N</i> -bromosuccinimide
nBuLi	n-butyl lithium
°C	degrees Celsius

OFETs	organic field-effect transistors
OLEDs	organic light emitting diodes
ppm	parts per million
PV	photovoltaic
s	singlet (NMR descriptor)
S	length of nominally single bond
$S\text{ cm}^{-1}$	conductivity
S-D	source-drain electrodes
Sp	selenophene
t	triplet (NMR descriptor)
T	thiophene
Torr	unit of pressure
Tz	thiazole
$\delta$	NMR chemical shift
$\Omega\text{ cm}$	resistivity



## List of Schemes

<i>Scheme 2.1</i> - Example of a Sandmeyer reaction.....	20
<i>Scheme 2.2</i> - Formation of nitrosonium ion.....	21
<i>Scheme 2.3</i> - Formation of benzenediazonium ion.....	21
<i>Scheme 2.4</i> - Catalytic cycle of the halogenation of diazonium salt.....	22
<i>Scheme 2.5</i> - Mechanism of 2-amino-4-hexyl-1,3-thiazole.....	23
<i>Scheme 2.6</i> - Synthesis of 2-amino-4-hexyl-1,3-thiazole <b>(1)</b> .....	24
<i>Scheme 2.7</i> - Synthesis of 2-bromo-4-hexyl-1,3-thiazole <b>(2)</b> .....	28
<i>Scheme 2.8</i> - Deamination of 2,2'-diamino-4,4'-bithiazole <b>(3)</b> .....	28
<i>Scheme 3.1</i> - Synthesis of 4-hexyl-2-methyl-1,3-thiazole <b>(4)</b> .....	33
<i>Scheme 3.2</i> - Synthesis of 5-bromo-4-hexyl-2-methyl-1,3-thiazole <b>(5)</b> .....	33
<i>Scheme 3.3</i> - Synthesis of Bromofuran <b>(6)</b> .....	34
<i>Scheme 3.4</i> - Synthesis of 2-(tributyltin)-furan <b>(7)</b> .....	34
<i>Scheme 3.5</i> - Synthesis of 2,2'-bis(2-thienyl)-4,4'-bithiazole <b>(8)</b> .....	36
<i>Scheme 3.6</i> - Synthesis of 2,2'-bis( <i>N</i> -pyrrolyl)-4,4'-bithiazole <b>(12)</b> .....	37
<i>Scheme 3.7</i> - Synthesis of 5-(4-hexyl-1,3-thiazolyl)-2,2':5',2"-terthiophene <b>(13)</b> .....	38
<i>Scheme 3.8</i> - Stille coupling of 5-(2-furanyl)-2,2':5,2"-terthiophene <b>(14)</b> .....	38
<i>Scheme 3.9</i> - Suzuki coupling of 5-(2-furanyl)-2,2':5,2"-terthiophene <b>(14)</b> .....	39
<i>Scheme 3.10</i> - Mechanism for Suzuki coupling reaction for compound <b>14</b> .....	41
<i>Scheme 4.1</i> - Aromatic vs quinoidal character.....	48
<i>Scheme 4.2</i> - Monomers.....	50
<i>Scheme 4.3</i> - Dimers.....	55
<i>Scheme 4.4</i> - Tetramers.....	65

## List of Figures

<i>Figure 1.1.</i> Schematic diagram of band gap of metals, semiconductors and insulators.....	1
<i>Figure 1.2.</i> A typical bilayer of an organic photovoltaic cell.....	6
<i>Figure 1.3.</i> Light absorption by an organic photovoltaic device.....	7
<i>Figure 1.4.</i> Construction of OLEDs.....	9
<i>Figure 1.5.</i> Schematic of an organic transistor, showing the injected static charge after application of a writing voltage as isolated monopoles (top) or as oriented dipoles (bottom).....	10
<i>Figure 1.6.</i> Examples of non-aromatic (cyclohexane) and aromatic hydrocarbons.....	12
<i>Figure 1.7.</i> Some examples of five-membered aromatic heterocyclic rings.....	12
<i>Figure 1.8.</i> The intermolecular N...H-C interaction between two thiazole rings.....	16
<i>Figure 1.9.</i> Oligomers containing aromatic rings.....	17
<i>Figure 1.10.</i> Thiazole-containing oligomers 1 and 2 previously synthesized by the MacKinnon group.....	18
<i>Figure 1.11.</i> Four-ring oligomer synthetic targets of this study.....	19
<i>Figure 2.1.</i> Attempted Sandmeyer reactions on 2-amino-4-hexyl-1,3-thiazole.....	26

## List of Tables

<i>Table 2.1.</i> Results of the Sandmeyer reaction on aniline substrate.....	26
<i>Table 3.1.</i> The Kumada synthesis of compounds <b>9</b> , <b>10</b> , and <b>11</b> .....	36
<i>Table 4.1.</i> $\omega$ B97XD/Def2TZVPP HOMO-LUMO energy/band gap, BLA, and effective localization index of the monomers.....	53
<i>Table 4.2.</i> $\omega$ B97XD/Def2TZVPP HOMO-LUMO energy/band gap of the dimers.....	58
<i>Table 4.3.</i> $\omega$ B97XD/Def2TZVPP bond length alternation ( $\text{\AA}$ ), conjugation between C-C bridge bond distance ( $\text{\AA}$ ) and localization index of dimers.....	63
<i>Table 4.4.</i> $\omega$ B97XD/Def2TZVPP HOMO-LUMO/energy gap (eV) of the tetramers.....	66
<i>Table 4.5.</i> $\omega$ B97XD/Def2TZVPP C-C bridging and their various bond length ( $\text{\AA}$ ) at different position of the tetramers.....	67
<i>Table 4.6.</i> $\omega$ B97XD/Def2TZVPP Bond length alternation and localization index of the tetramers.....	68

# Chapter 1-Introduction

## 1.1 Semiconductivity

Semiconductors are required for the operation of a variety of modern electronic devices. For example, light-emitting diodes (LEDs) and photovoltaic (PV) devices convert between light and voltage using a semiconductor. A semiconductor is usually defined as a material with electrical resistivity lying in the region of  $10^{-2}$ – $10^9 \Omega \text{ cm}$ .<sup>1</sup> Alternatively, it can be defined as a material whose energy-gap between the valence band and the conduction band for electronic excitations lies between zero and about four electron volts (0-4 eV) as shown in Figure 1.1.

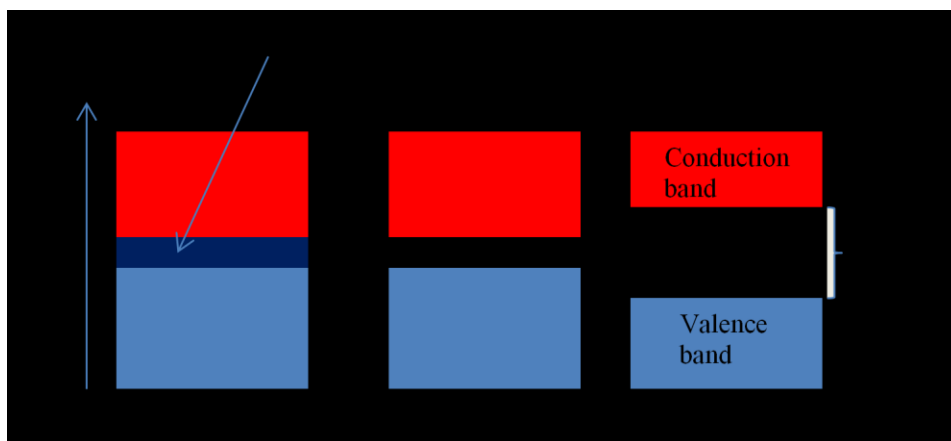


**Figure 1.1: Schematic diagram of band gaps for metals, semiconductors and insulators**

Materials with a zero energy gap are metals, while those with an energy gap larger than 4 eV are more frequently known as insulators. There are frequent exceptions to this generalization, for example, boron-doped diamond is often used as a ‘wide band gap semiconductor’, with an energy gap of about 6 eV. Traditional inorganic semiconductors are divided into elemental and compound types. Good examples of the elemental type are germanium, selenium, carbon (in the form of  $C_{60}$ ), and silicon, which is undoubtedly the best known semiconductor. Commonly-used

compound semiconductors include gallium arsenide, aluminium phosphide, aluminium arsenide, and indium phosphide (with a 1.5 eV energy gap).<sup>1</sup>

A metal has no electronic energy barrier because the valence band and the conduction band overlap, thereby allowing the electrons to move freely throughout the solid; there is no energetic barrier of activation between the valence and conduction band. In an insulator, there is a high energy gap (4 eV) between the valence and conduction band, so potential charge carriers do not have enough energy to overcome the band gap under normal conditions of temperature and pressure. In semiconductors, the intermediate energy gaps allows the promotion of some electrons by either photoexcitation or heat to cause the electrons to move from the valence band to the conduction band as shown in Figure 1.1

The band gap can be changed through doping. In this doping process, the number of holes and the number of excited electrons are equal:  $n = p$ , where  $n$  equals the number of generated free electrons in the conduction band and  $p$  is the number of vacancies (holes) left behind in the valence band. Such semiconductors can be divided into  $n$ -type and  $p$ -type, where the charge carriers are negative (electrons in the conduction band) or positive (holes in the valence band), respectively. Addition of impurities, either deliberate (called “doping”) or unintentional, can create extra electrons or holes in the electronic structure. Conversely,  $p$ -type doping generates acceptor impurities, resulting in electrons moving from the valence band to the acceptor level. These results in hole-mobility in the valence band. The addition of gallium or boron impurities to intrinsic silicon will create this type of semiconductor.<sup>2</sup> In any semiconducting or insulating material, the conductivity increases as a result of increasing the number of charge carriers generated by supplying energy to overcome the band gap. If the mobility value of the charge carrier is high, it promotes fast device operation, which is needed

for low cost electronics. The mobility of charge carriers can have a limiting effect. Once generated, the mobility of the charge carriers will decrease with increasing temperature, just as they do for a metallic conductor, and for the same reason (mean free path of the charge carriers decreases due to increased number of thermal collisions). This limitation is encountered in semiconductors because an increase in temperature causes the number of charge carriers to increase.

## 1.2 Introduction to molecular semiconductors

Organic electronics are an emerging technology with great promise for convenient, innovative, and high performance electronics. In the late 1970s, it was discovered that plastics, which are intrinsic insulators, could be made to be conductive upon modification. This discovery gave rise to the modern field of organic electronics. Over the years, organic semiconductors have been a subject of academic and commercial interest as an alternative to inorganic semiconductors. Organic semiconductors have several advantages over their inorganic counterparts such as lower power requirements, lower cost of production, lighter weight, and flexibility in the fabricated devices. The main advantage of organic semiconductors is that they can be assembled onto a fully flexible substrate, or to assemble the entire structure with no substrate at all. It is possible to then expose the gate side of such a film to an external medium to apply to any kind of substrate.<sup>3</sup> Some of the disadvantages of molecular semiconductors compared to their inorganic counterparts include complexity of synthesis, lower temperature tolerance, shorter lifetimes, and lower performance in high-end devices such as computer chips, due to degradation under environmental influences. For example, thin-film organic field-effect transistors (OFETs) made from pentacene have a high electron mobility of  $3.0 \text{ cm}^2 \text{ V s}^{-1}$  but are unstable in air and processing is difficult due to their very low solubility in solvent.<sup>4</sup> On the other

hand, some technologies using organics are fully matured and commercially available, *e.g.* organic light-emitting diode (OLED) televisions are readily available at any department store.

Organic semiconductors are  $\pi$  conjugated molecular or polymeric compounds in which charge carriers migrate under the influence of an electric field. Like their inorganic counterparts, organic semiconductors can be classified as *n*-type or *p*-type.<sup>5</sup> Because of the strong localization of electrons in organic molecules, the solid-state bands are narrow. They arise from the highest occupied molecular orbital (HOMO) and the lowest unoccupied molecular orbital (LUMO), giving rise to the valence and conduction bands, respectively. The HOMO will be a bonding or non-bonding (lone pair) orbital containing electrons, while the LUMO is empty and usually antibonding. The difference in energy between the HOMO and LUMO is the lowest energy electronic excitation that is possible in the molecule. The band gap in the solid will be slightly smaller than the HOMO-LUMO gap due to the width of the bands, but because the bands are so narrow in organic solids, the HOMO-LUMO gap ( $E_{\text{H-L}}$ ) will be very similar to the band gap,  $E_{\text{g}}$ . An extended  $\pi$ -structure is needed in organic semiconductors to cause the band gap to come into the semiconducting range. These molecules are also flat, yielding tightly-packed solid state structures: a necessity because the electron transport occurs through hopping from  $\pi$ -system to  $\pi$ -system in organic systems, and the shortest distance between  $\pi$ -systems will occur when the molecules are arranged in  $\pi$ -stacks.<sup>5</sup>

### 1.2.1 Current strategies for the production of organic semiconductors

Hydrocarbon materials are typically *p*-type semiconductors. Incorporating a functional group as a substituent on a  $\pi$ -conjugated system can be used to change parameters such as HOMO-LUMO gap, absolute energies of the HOMO and LUMO, type of conductivity (*p*, *n*, or ambipolar), processing characteristics (*e.g.* solubility for solution processing), adhesion to

substrate, etc. This approach, often called tuning, can produce high performing materials with the appropriate energy level and strong and broad absorption spectra.<sup>6</sup> Examples of electron accepting groups that might be affixed to the molecule for the purposes of tuning include cyano, carbonyl, perfluoroalkyl, and amids. Some electron-donating groups are oligothiophenes, triarylamine, porphyrin, and fused thiophene. Introducing electron-withdrawing groups in a  $\pi$ -conjugated semiconductor will generally lower the lowest unoccupied molecular orbital (LUMO) energy because the  $\pi^*$ -energy of the electron-withdrawing group is closer to the LUMO of the  $\pi$ -conjugated entity and that leads to the stabilization of the LUMO.<sup>5</sup>

The aromatic rings that make up the  $\pi$ -system of the main chain rings can also be divided into electron-donating and electron-withdrawing. The most common rings are *p*-type with electron-rich (donating) rings, such as thiophene and benzene. Electron-poor rings should move the molecule towards *n*-type character. Thiazole, for example, is an electron accepting heterocyclic compound because of the electron-withdrawing ability of the imine (C=N).<sup>6,7,8</sup>

### **1.2.2. Application of organic semiconductors**

Organic semiconductors have been utilized in myriad applications.<sup>9</sup> Rapid growth in organic electronics has offered several newer areas of application with improved stability, long life, better performance, and reproducibility as demanded by the different sectors where they find their uses. Organic semiconductors are used as an alternative to inorganic semiconductors in areas as diverse as organic photovoltaic devices (OPVs), organic light-emitting diodes (OLEDs), and organic field-effect transistors (OFETs). This section provides examples of organic semiconductors used in the above mentioned applications.



### 1.2.2.1 Organic photovoltaic cells

Organic semiconductors can be used in photovoltaic solar cells, which are used to convert solar energy to electrical energy. The organic material, in the form of a polymer, oligomer, dendrimer, dye, or pigment, can be used as the active material or in conjunction with a silicon-based material.<sup>9</sup> A typical OPV device consists of one or several photoactive materials sandwiched between two electrodes. A typical bilayer (two semiconducting layers) organic photovoltaic device is shown in Figure 1.2.

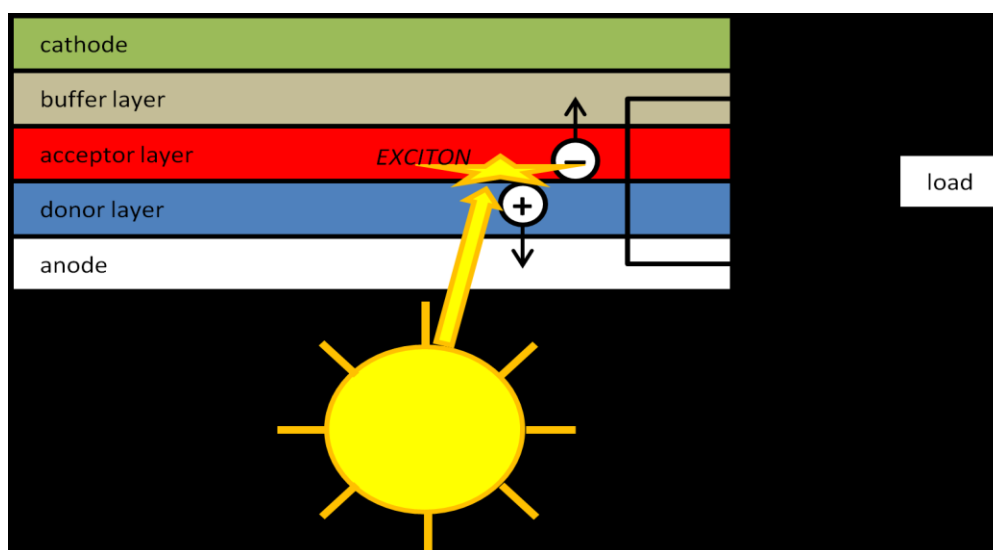


**Figure 1.2. Structure of a bilayer of an organic photovoltaic cell**

In this device, sunlight is absorbed in the photoactive layers, which is composed of donor and acceptor semiconducting organic materials to generate photocurrents. As shown in Figure 1.3, those photoactive materials harvest photons from sunlight to form excitons, in which electrons are excited from the valence band into the conduction band. The excitons migrate to the donor-acceptor interface where they separate into free holes and electrons, in a process called

separation. A photocurrent is generated when the holes and electrons move to the corresponding electrodes.

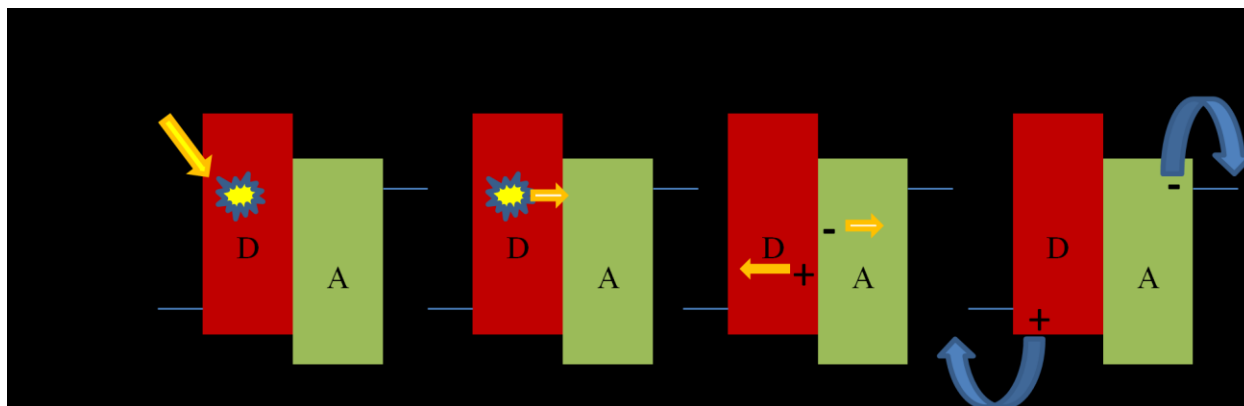


**Figure 1.3. Light absorption by an organic photovoltaic device**

Wuhlbacher and Scharber reported that MEH-PPV, poly[2-methoxy-5-(2-ethylhexyloxy)-1,4-phenylenevinylene], can be used as an electron donor in solar cells. It has an absorption edge of 550 nm, which corresponds to a band gap of 2.3 eV. When they compared MEH-PPV with P3HT, a derivative of poly(3-alkyl-thiophene), they realized P3HT exhibited a lower and broader absorption band, a better hole mobility and better donating ability when blended with phenyl-C<sub>61</sub> butyric methyl ester, PCBM. PCBM blended with P3HT exhibited excellent photovoltaic properties.<sup>10</sup> Additionally, Kumaresan *et al.* demonstrated that fused thiophene-based material can be used alone in organic photovoltaics and in dye-sensitized solar cells to give low-cost photovoltaic devices at reasonable efficiencies.<sup>11</sup> The current record holder for a solar cell containing an organic material as the active layer(s) has a synthetically complex organic compound combined with a fullerene to give an overall power conversion efficiency of 17.3%.<sup>12</sup>

Diketopyrrolopyrrole (DPP) has also been exploited by Qu *et al.* for a photovoltaic application.<sup>13</sup> They indicated that thiophene-connected DPP showed a low band gap and a high photocurrent density due to the broad absorption spectra. They demonstrated that by tuning the HOMO-LUMO energy levels by connecting different electron donor moieties they enhanced the power conversion efficiency. They also noted that DPP moieties joined with furans and thienothiophene showed excellent photovoltaic properties. Furthermore, Fernandes *et al.* reported the synthesis and characterization of a push-pull interaction between a bithiophene and thienothiophene bearing an ethyne linker as sensitizer for dye-sensitized solar cells. The push-pull (donor-acceptor) dyes are generally added to increase charge separation, thus creating charge carriers. They studied the effect of different  $\pi$ -bridging units of ethynyl-thienothiophene and ethynyl-2,2'-bithiophene with *N,N'*-dimethylaniline as a donor moiety. The better performance of their dye was ascribed to a higher photocurrent resulting from having bithiophene as  $\pi$ -bridge rather than the thienothiophene spacer. Bithiophene has a higher molar extinction coefficient, which is advantageous for light harvesting as compared to the thienothiophene. The  $\pi$ -bridge or spacers such as bithiophene provides excellent optoelectronic properties such as efficient  $\pi$ -conjugation, low geometric relaxation energy upon oxidation, and increased planarity.<sup>14</sup> Thiophene oligomers are more planar than their phenyl analogues because of the anti configuration of bithiophene; there is no steric interaction between the H-atoms on neighbouring rings, which is not the case in biphenyl.

#### **1.2.2.2. Organic light-emitting diodes (OLEDs)**

Most organic molecules or polymers having a  $\pi$ -conjugated heteroaromatic backbone transport charges and efficiently interact with light and as such can be used as semiconductors in optoelectronic devices, comparable to their inorganic counterparts. When a voltage is applied

across the OLED, current flows from the cathode to the anode. The cathode injects electrons into the emissive layer. The anode removes electrons from the conduction layer and at the boundary between the emissive and conductive layer, electrons and holes recombine with a consequent release of energy in the form of a photon.

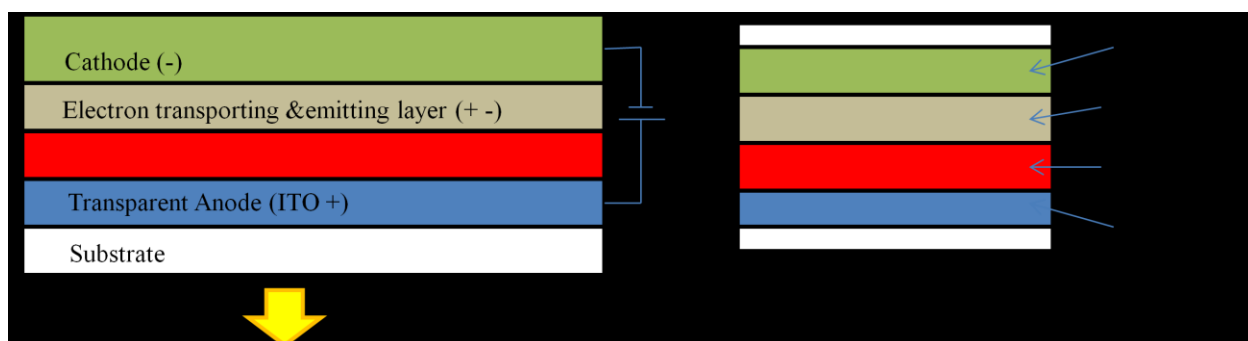


**Figure 1.4: Construction of OLEDS**

Muller *et al.* reported in a three-colour, that is red-green-blue, OLED using polymers. They used photoresistive starting materials that would polymerize when photochemically initiated (e.g. from oxetane side groups) to allow selective polymerization in a preferred area.<sup>15</sup> Another key example is Gross *et al.*'s use of poly(3,4-ethylenedioxythiophene) PEDOT), to produce devices with bright colours and low energy consumption.<sup>16</sup>

### 1.2.2.3 Organic field-effect transistors (OFETs)

An OFET is not optoelectronic – its charge carriers are generated by voltage and is inexpensive compared to inorganic counterparts. As shown in Figure 1.5, a thin film of organic semiconductor is deposited on top of a dielectric with underlying gates. Charge-injection source-drain (S-D) electrodes which provides the contact are defined on top of the organic semiconductor and this gives the top-contact configuration on the surface of the substrate before the deposition of the semiconductor film, which gives the bottom-contact configuration. The top-

contact configuration has the charge-injecting source-drain (S-D) electrodes on top of the organic semiconductor. Electrodes located on the substrate, which later has the organic semiconductor deposited on it, gives the bottom-contact configuration.

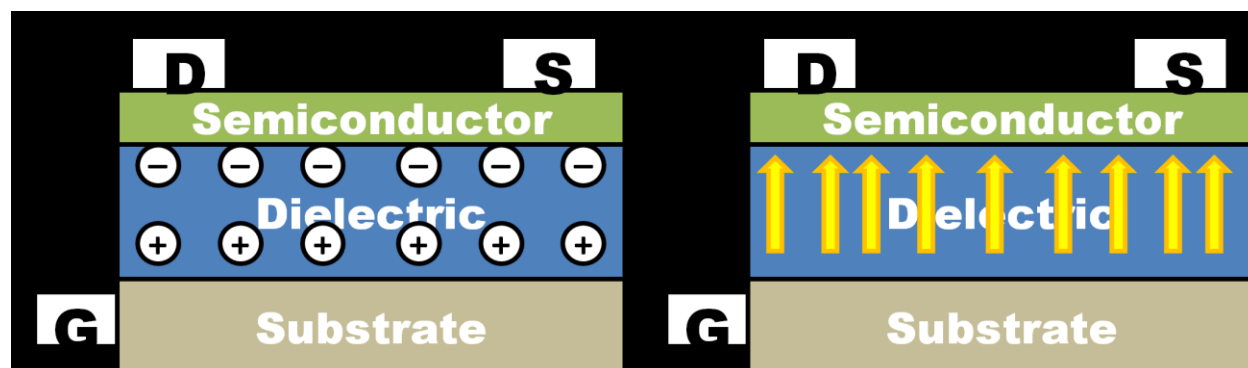


**Figure 1.5: Schematic of an organic transistor, showing the injected static charge after application of a writing voltage as isolated monopoles (top) or as oriented dipoles (bottom)**

To achieve optimal performance in an OFET, the HOMO and LUMO energies of the semiconducting molecules must be at a level where the holes or electrons can be induced when an electric field is applied. In addition, there must be sufficient overlap of the frontier orbitals on neighbouring molecules to allow efficient migration of charges between them. Furthermore, the organic material should be pure to prevent impurities from acting as charge carrier traps. Lastly, the organic molecules should be oriented with their longest axis perpendicular to the substrate of the field effect transistor. The charge carriers migrate by hopping between  $\pi$ -systems, so those  $\pi$ -systems must be oriented at such to maximize electron mobility.<sup>17</sup>

In one systematic study of materials for field-effect devices, Ying *et al.*<sup>18</sup> demonstrated the design and synthesis of fused thiophenes and their derivatives. The fused thiophenes showed excellent field effect characteristics due to intermolecular interaction between the sulfurs (S $\cdots$ S) and  $\pi$ - $\pi$  stacking. Of all their examples, T1-T8 (T1 is one thiophene and T8 is eight thiophene

rings fused together), T5 was the most attractive for OFET applications because their molecules were arranged with their long axes, electron mobility of  $0.045 \text{ cm}^2 \text{ V}^{-1} \text{ s}^{-1}$  and an  $I_{\text{on/off}}$  ratio of  $10^3$  was obtained when they were tested in air, and they had a large band gap of 3.29 eV. The longer molecules 'fell over' and so were parallel to the substrate. This result indicates that materials based on the thiophene-fused system are promising organic materials for use in OFETs.<sup>18</sup>

### 1.3 Hetero(aromatic) compounds

This section is a discussion about the specific molecules that make up organic semiconductors, and why heteroaromatic compounds are especially interesting research targets. Pentacene ( $\text{C}_{22}\text{H}_{14}$ ), (Figure 1.6), a polycyclic aromatic hydrocarbon consisting of five linearly-fused benzene rings, is often considered the 'gold standard' in organic semiconductors. It can be fluorinated to give perfluoropentacene without disrupting the aromaticity, as depicted in Figure 1.6, turning it into an *n*-type semiconductor.<sup>19</sup>

The term "aromatic" refers to conjugated ring systems containing  $4n+2$   $\pi$ -electrons. Thus, the 6-membered cyclohexane ring  $\text{C}_6\text{H}_{12}$  with 0  $\pi$ -electrons is not aromatic (and is not planar in three dimensions, in spite of how it is often represented), while the benzene ring  $\text{C}_6\text{H}_6$  with six  $\pi$ -electrons is aromatic. Correct substitution with heteroatoms can maintain the aromatic character. For example exchanging C-H with N gives pyridine, which is also aromatic as depicted in Figure 1.6

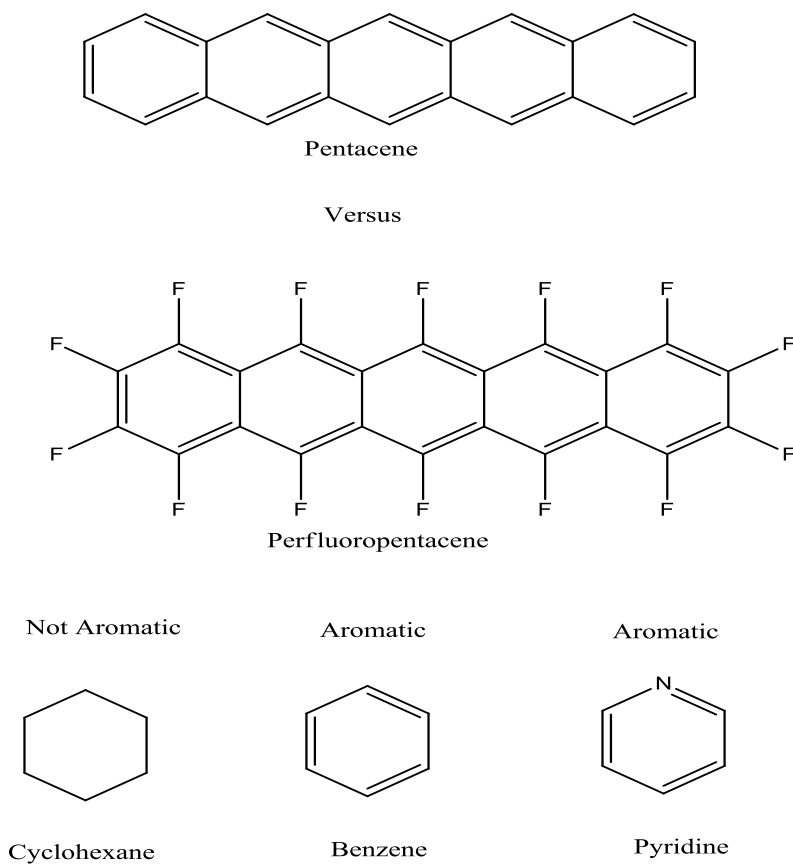


**Figure 1.6: Examples of non-aromatic (cyclohexane) and aromatic hydrocarbons**

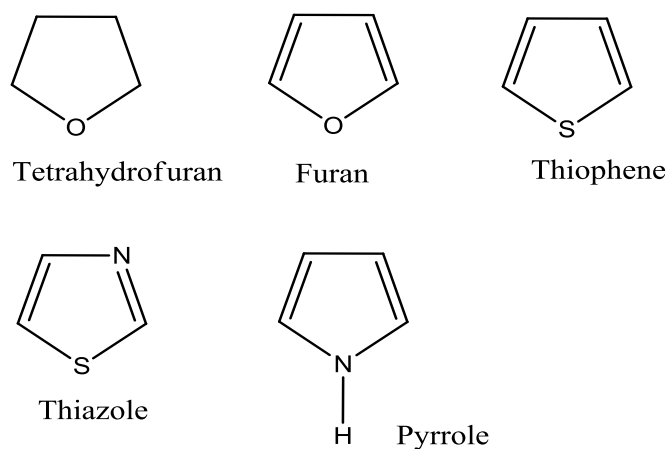


**Figure 1.7: Some examples of five-membered non aromatic (tetrahydrofuran) and aromatic heterocyclic rings**

### 1.3.1 Heteroatoms

Five-membered rings can also be aromatic if they include a heteroatomic unit that donates two  $\pi$ -electrons to the ring system (or if a charge is added, such as in the case of cyclopentadienyl  $C_5H_5^-$ ). Examples are shown in Figure 1.7, showing moieties such as chalcogens or Pn-H (where Pn is a pnictogen).<sup>20,21</sup>

### 1.3.2 Chalcogenophenes

Chalcogenophenes (furan, thiophene, selenophene, tellurophene) are 5-membered aromatic rings  $C_4H_4X$ , where X is one of the Group-16 elements. Each of these four ring systems has been investigated for use in field effect transistors and organic photovoltaic materials, and has shown different electrochemical properties.<sup>9,10,11,16</sup>

#### 1.3.2.1 Oligothiophenes

Oligothiophenes have attracted a strong interest among researchers the world over and have been the most frequently used  $\pi$ -conjugated materials as the main components in organic electronic devices and molecular electronics.<sup>22</sup> Lately, the traditional linear systems have been extended to higher dimensionalities and new topologies have been synthesized and various functional molecular designs have been characterised with thiophene rings as the base. Thiophene chemistry has been established and developed for a long time and there are various ways to derivatize the core molecule. Thiophenes have special redox, optical, and electronic properties as well as average self-assembling properties on solid surfaces. Thiophenes allow fine tuning of desirable properties and it is easier to get them into  $\pi$ -stacks than acenes because they have fewer C-H bonds that prefer the T-shaped C-H $\cdots\pi$ -cloud interaction. The sulfur atom in the ring has high polarizability, which makes the molecule more stable during charge transport, a property that is vital for molecular and organic electronics. Oxidation is a potential weakness of



thiophenes (although you can use S,S-dioxothiophene as a molecular material too).<sup>23</sup> Thiophenes can be functionalized in positions  $\alpha$  and  $\beta$  to sulfur, but because of the difference in reactivity, regioregular oligomers with varied functionalities can be prepared and characterized. The oligomers can be linear, branched, or dendrimeric. Thiophene is a cheap starting material, being obtainable as a by-product of petroleum distillation.<sup>24</sup>

Tuning of the electronic properties of organic semiconductors can be done through modification of the constituent molecules. Garnier *et al.*<sup>25,26</sup> reported that increasing the conjugation length of well-defined conjugated thiophene oligomer leads to a spectacular increase in charge transport properties as expressed by the high carrier mobility observed in field-effect transistors based on sexithiophene (6T).

Further modification of the oligothiophene core has led to further improvements. When alkyl groups are attached to the end of 6T, they allowed them to control the mesoscopic organization of the molecules by increasing the molecular organization, which gave highly ordered thin films with improved charge transport, as indicated by a large anisotropy in the conductivity of a thin-film transistor devices and a high carrier mobility ( $10^{-5}$ - $10^{-4}$  cm<sup>2</sup> V<sup>-1</sup> s<sup>-1</sup>).<sup>27</sup> Barclay *et al.* showed that  $\pi$ -stacking could be reliably induced in oligothiophenes (which normally pack in a herringbone fashion) by the attachment of terminal cyano groups.<sup>28,29,30</sup> Pickup *et al.* reported on the electronic interaction between a metal centre and conjugated bithiophenes.<sup>31</sup>

Substitution can change the semiconductor from *p*-type to *n*-type. Facchetti<sup>32</sup> did this by changing the dihexylsexithiophene (DH-6T) (a *p*-type semiconductor) to perfluorohexyl to give  $\alpha,\omega$ -diperfluorohexylsexithiophene (DFH-6T), an *n*-type semiconductor. Differential scanning

calorimetry and thermal gravimetric analysis were used to find the comparable thermal properties between the two compounds. DFH-6T showed a crystal-to-liquid crystal transition at 292 °C and an isotropic transition at 309 °C whereas DH-6T showed a crystal-to-liquid crystal transition at 300 °C. They concluded that the two compounds have similar thermal characteristics and identical melting points, which was an indication that the strong  $\pi$ - $\pi$  interaction of DH-6T is preserved upon substitution with the fluoroalkyl groups.

### 1.3.2.2 Oligoselenophene

Oligoselenophenes have been used as active layers in organic field effect transistors. They have similar physical, chemical, and semiconducting properties as thiophenes. Although their electrical conductivity is only in the range of  $10^{-4}$ - $10^{-2}$  S  $\text{cm}^{-1}$ , which is very small in comparison with intrinsic oligothiophenes, they have some advantages over thiophene based organic semiconductors. Polyselenophenes have a smaller optical band gap because the polymer backbone is more planar than thiophenes due to the shorter C-C bonds between the selenophene rings in the same molecule. Selenophene-based compounds have stronger intermolecular interactions than the thiophene-based molecules due to the fact that selenium is more easily polarized than sulfur, and the selenium is a physically larger atom.<sup>33,34</sup>

### 1.3.2.3 Oligofuran

Oligofurans are relatively new compounds due to the difficulty in synthesizing them. Oligofurans containing up to nine rings have been synthesised by Bendikov *et al.*<sup>35</sup> They found them to be more thermally stable, to have greater solubility, and to have a tighter herringbone packing than the equivalent oligothiophenes. Gidron *et al.* prepared oligofuran-based materials for organic field effect transistors that have good charge mobility and a better on/off ratio

compared to their oligothiophene counterparts, as well as excellent electroluminescent properties, even in non-optimized LED devices.<sup>36</sup>

### 1.3.2.4 Thiazole

Compared to oligothiophenes, selenophenes, and phenyls,<sup>37</sup> very little has been done to investigate optoelectronic properties of oligothiazoles. Usta *et al.*<sup>38</sup> reported the synthesis of a bithiazole and an electron-withdrawing perfluoroalkyl chain to alter the electron transport characteristics of the resulting copolymer. They showed that thiazoles have some promising characteristics as a semiconductor building block, in comparison with their thiophene-based counterparts. They concluded that thiazoles have lower LUMO energies for electron stabilization (0.2-0.3 eV) as compared to thiophenes, they have a very large dipole moment, which helps in the alignment of the molecule (1.61 D for thiazole and 0.52 D for thiophene), and they have non-bonded intermolecular interactions, between "N-S" and N-H-C, which helps in the planarity of the compound.

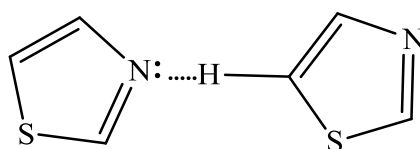


**Figure 1.8: The intermolecular N...H-C interaction between two thiazole rings**

## 1.4 Computational Studies

From the earliest crude computational models using MNDO (Modified Neglect of Diatomic Overlap)<sup>23, 39</sup> to the most recent DFT (Density Functional Theory) levels of theory,<sup>40</sup> materials chemists have been using *ab initio* calculations to understand oligomeric semiconductors and to design improvements. These calculations are becoming more and more

powerful as computing power becomes faster and cheaper. Unfortunately, the added power and flexibility adds a myriad of choices of parameters to model, so a judicious choice is required in modelling materials systems. These models and choices will be detailed in the introduction to Chapter 4.

## 1.5 Scope of Thesis

Oligomers containing aromatic rings such as oligothiophenes, oligophenyl, and oligo(phenylenevinylene),<sup>41</sup> are organic materials with current interest for use in organic electronics (Figure 1.8). All these materials can act as wide band gap semiconductors, many examples emit light when a voltage is applied, and they can be modified to tune the band gap, which changes the colour or the type of charge carrier (these three are *p*-type, but with the addition of electron-withdrawing groups, they can become *n*-type).<sup>42</sup>

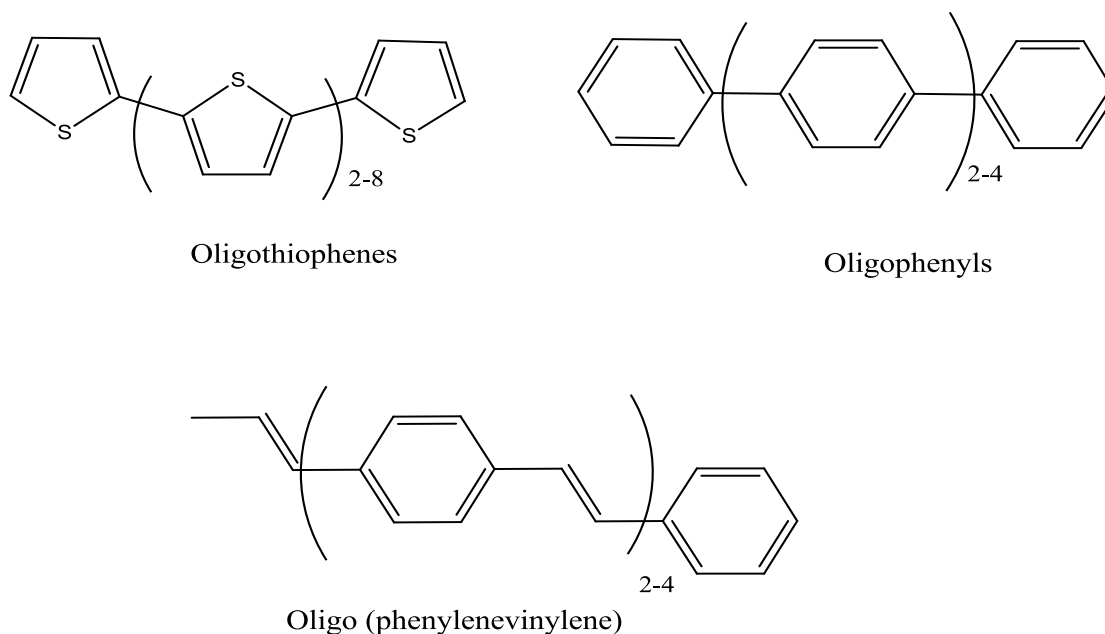
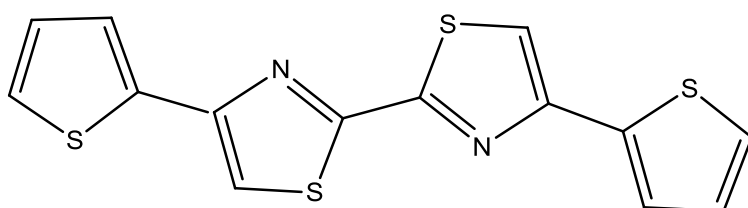
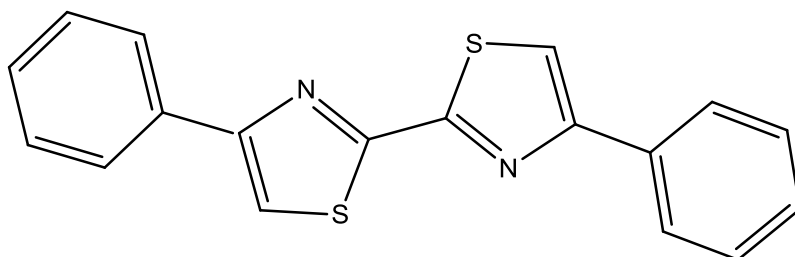


**Figure 1.8: Oligomers containing aromatic rings**

This study aimed to investigate the design of new synthetic methods for the creation of oligomeric semiconductors containing heterocyclic rings, and a parallel computational study on the same new systems. Specifically, we were interested in replacing one or more thiophene rings with different heterocyclic rings such as thiazole or furan rather than looking at the substituent effects for electronic tuning. The Mackinnon group had previously prepared the following two species, Figure 1.9



**4,4'-di(2-thienyl)-2,2'-bithiazole ( $T_2Tz_2$ )**



**4,4'-diphenyl-2,2'-bithiazole ( $Ph_2Tz_2$ )**

**Figure 1.9: Thiazole-containing oligomers 1 and 2 previously synthesized by the MacKinnon group**

In this thesis, we have investigated synthetic routes to thiophene-thiazole, thiophene-*N*-pyrrole, and thiophene-furan mixed heterocyclic oligomers. Figure 1.11 shows the structures of the oligomers that were our synthetic targets. Through DFT calculations on representative dimers and tetramers, we determined the electronic differences between oligomers containing one ring

type with those where at least one of the rings is replaced by an aromatic ring of another type.

Below are the four-ring oligomer synthetic targets of this study.

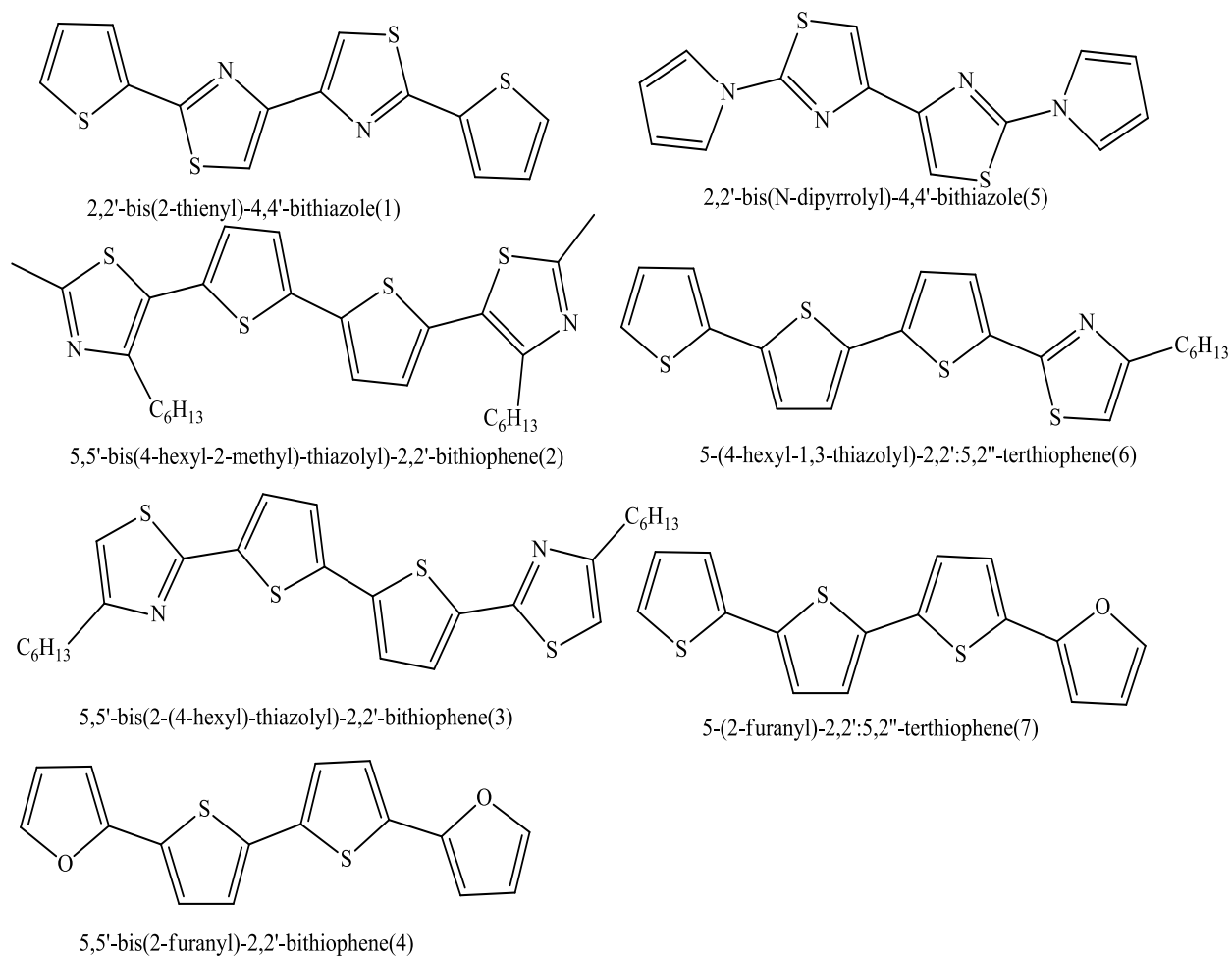


**Figure 1.10: Four-ring oligomer synthetic targets of this study**

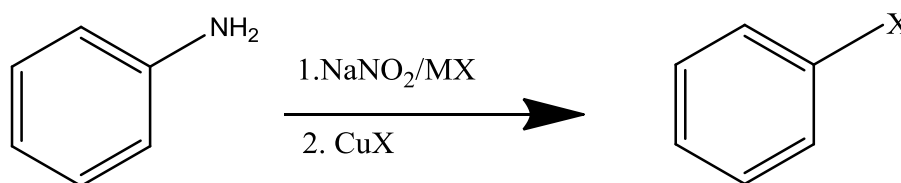
## Chapter 2-Sandmeyer reactions with heterocycles

### 2.1 Introduction

There are a number of ways to access the thiazole ring. One inexpensive and versatile method yields an amine-substituted ring. It was recognized that this precursor would be more versatile if a route was available to substitute the amine group for either a halogen or a hydrogen atom. One such method is the Sandmeyer reaction.

#### 2.1.1 The Sandmeyer reaction

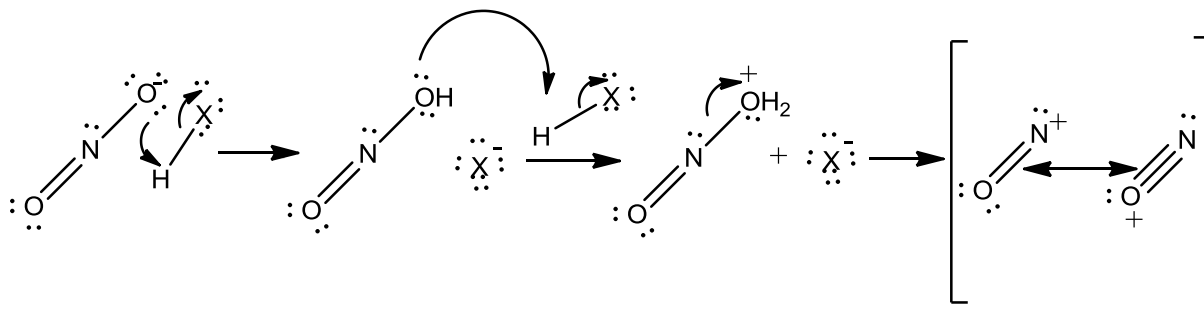
The Sandmeyer reaction is a substitution of an aromatic amino group for a halogen or pseudohalogen such as chloro, bromo, or cyano (Scheme 2.1). The conditions can also be used for deamination (substitution with H). The generally accepted mechanism using an inorganic nitrite source starts with the generation of a nitrosonium ion (Scheme 2.2), which proceeds to form an aromatic diazonium (Scheme 2.3). Finally, the diazonium leaving group is displaced by the incoming nucleophile (Scheme 2.4).<sup>43</sup>



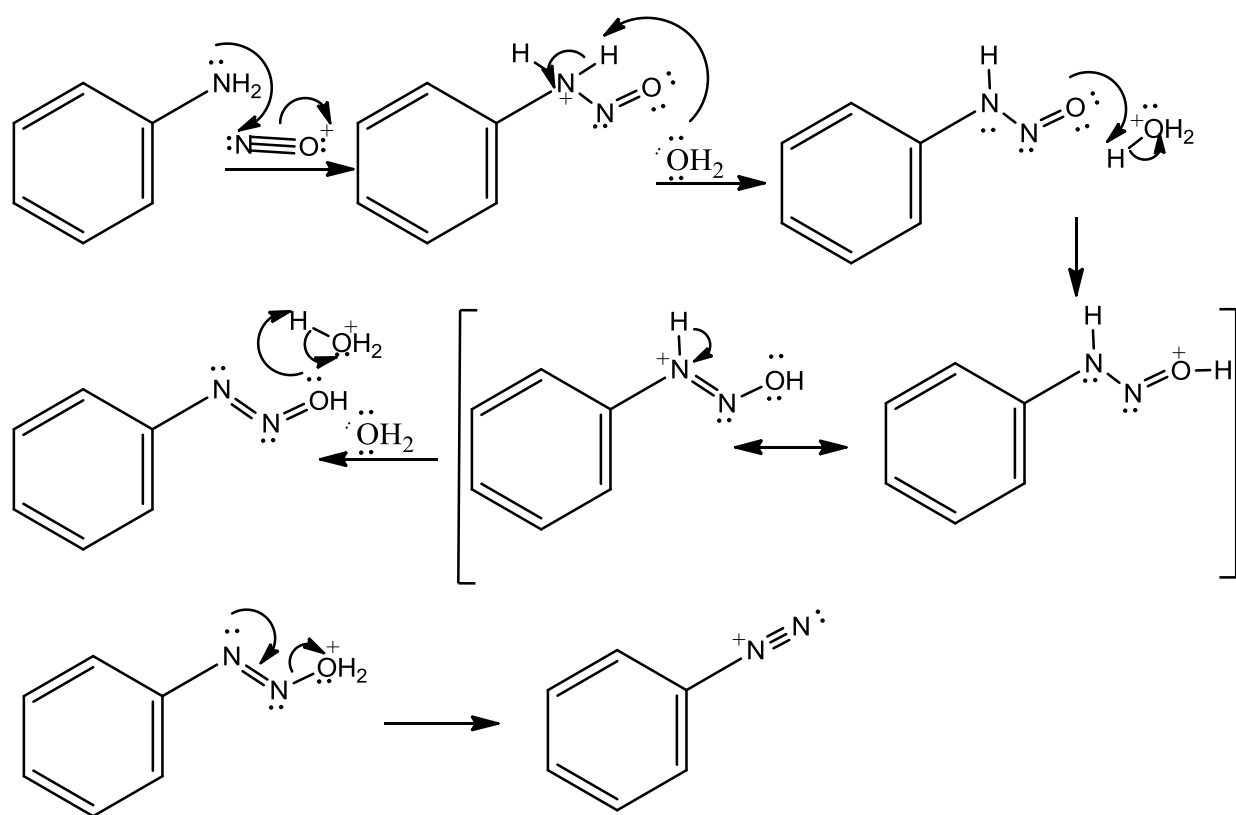
**Scheme 2.1: Example of a Sandmeyer reaction**

The X in Scheme 2.1 can be any halogen except F<sup>-</sup>, or a pseudohalogen such as CN<sup>-</sup>

Scheme 2.2: Formation of nitrosonium ion

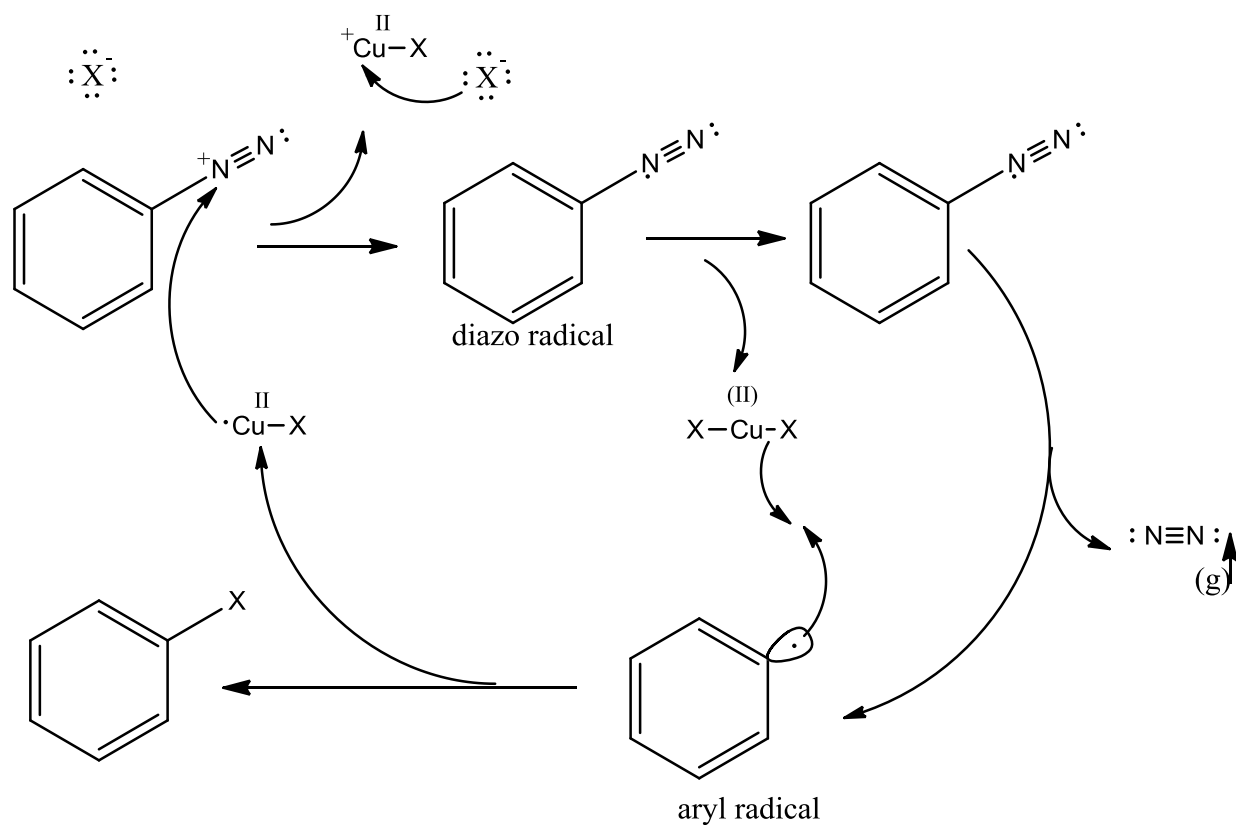


Scheme 2.3: Formation of benzenediazonium ion





**Scheme 2.4: Catalytic cycle of the halogenation of diazonium salt**

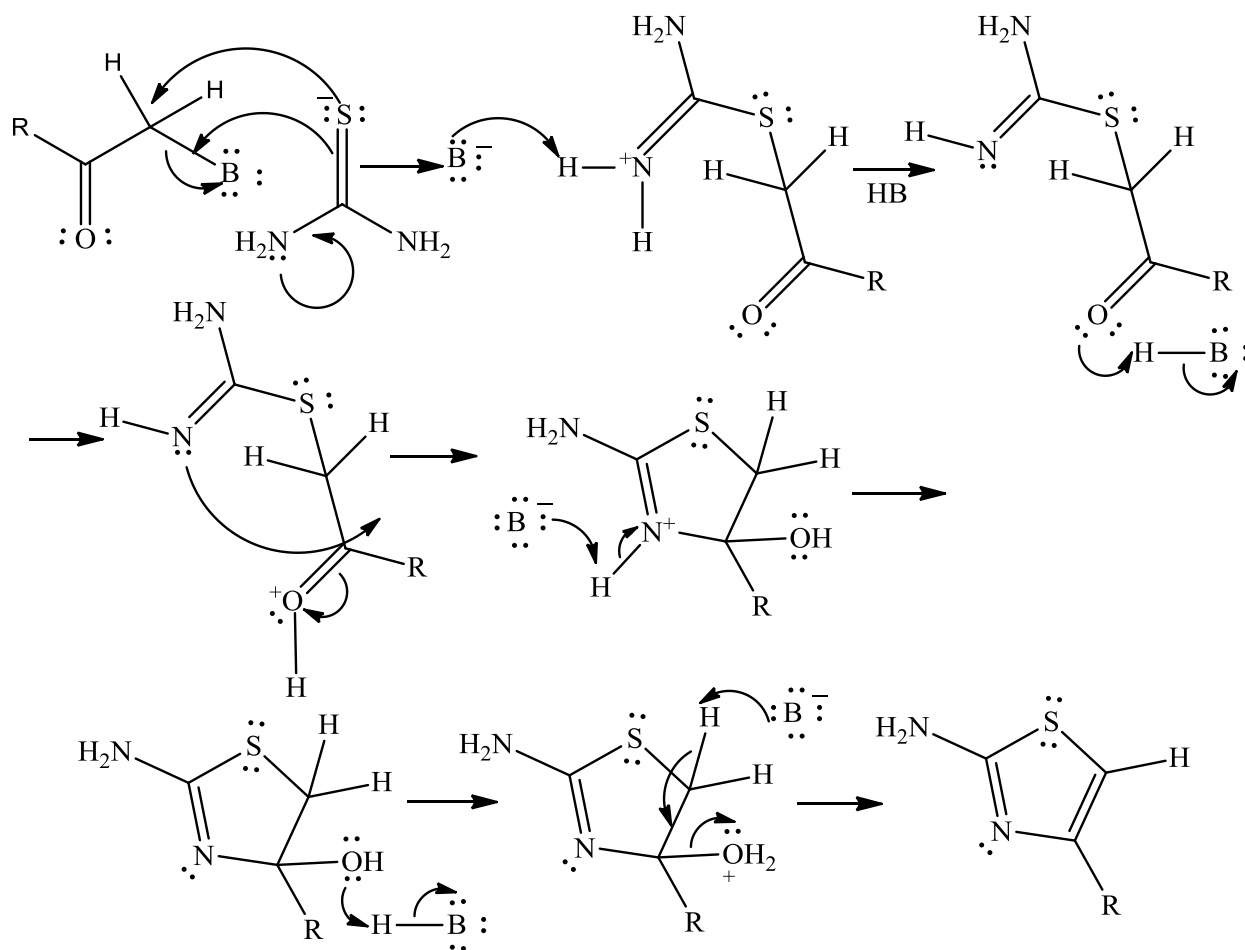


### 2.1.2 The Hantzsch thiazole synthesis

The thiazole ring can be conveniently prepared by the reaction of a thioamide with a 1-halo-2-ketone. The substituent on the thioamide becomes a substituent on the resulting thiazole ring at the 2-position (between the N and S), while the ketone substituent takes up the other position  $\alpha$ - to the nitrogen. The results are summarized by the mechanism proposed by Hantzsch, Scheme 2.5.

There are several inexpensive and readily available thioamides such as thioacetamide and thiourea. The advantage of the latter is that the resulting thiazole ring contains an amine group that can be substituted *via* the Sandmeyer reaction.

**Scheme 2.5: Mechanism of the formation of 2-amino-4-hexyl-1,3-thiazole (R and B are the hexyl group and the base)**



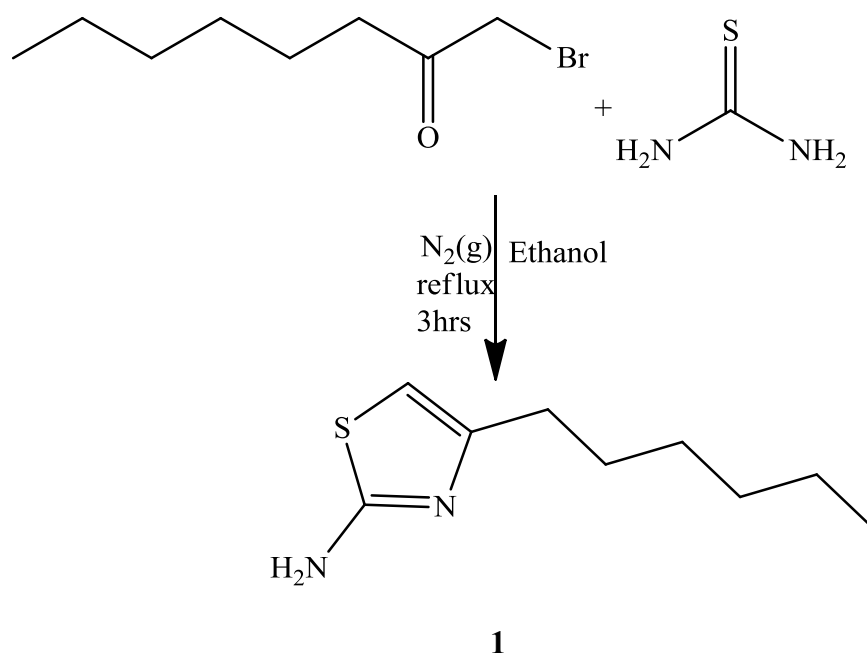
## 2.2 Results and discussion

### 2.2.1 Synthesis of 2-amino-4-hexyl-1,3-thiazole

Upon investigation of the literature, it was found that Sandmeyer reaction does not appear to have been attempted on thiazole rings. In fact, it has rarely been used in heterocyclic chemistry. We chose to use 2-bromooctanone as our haloketone for the prosaic purposes that it is easily synthesized and purified from bromine and 2-octanone (which is itself inexpensive), and that its lower volatility reduces the notorious lachrymatory effect of the 1-halo-2-ketone unit (2-

chloroacetone was a commercially available anti-riot and chemical warfare tear gas agent only replaced because the material had long-term storage issues that reduced its effectiveness). The bromine is selectively placed at the alpha position of the ketone due to the ability of the ketone to form enols in acidic solution. In acidic solution, usually only one alpha hydrogen is replaced by a halogen, because each successive halogenation is slower than the first. The halogen decreases the basicity of the carbonyl oxygen, thus making protonation less favorable.<sup>44,45</sup> The material was also purified by fractional (vacuum) distillation prior to use. The bromooctanone was reacted with thiourea to form the title compound 2-amino-4-hexyl-1,3-thiazole as shown in Scheme 2.6 (compound **1**).

**Scheme 2.6: Synthesis of 2-amino-4-hexyl-1,3-thiazole**



An additional advantage to this material, as we discovered, is that the resulting 2-amino-4-hexyl-1,3-thiazole is easily purified by vacuum distillation. The material then solidifies when pure to form a pale yellow solid that is straightforward to manipulate.

### 2.2.2 Comparative analysis of Sandmeyer reactions

There are very few examples in the literature of Sandmeyer reactions on heteroaromatic amines, and none (that we could find) on an aminothiazole. Therefore, we set out to determine the best set of conditions for our ring system. Multiple variations are possible, but we chose to investigate three nitrites (sodium nitrite, butylnitrite, and *tert*-butylnitrite), solvent (water, acetonitrile), and nucleophile source salt (copper (I) and (II) bromide, etc.). We first performed all reactions on aniline in order to have a baseline comparison. As expected, most of the reactions worked with aniline, as shown in Table 2.1. There were some notable exceptions (*e.g.* KCl seems to be a particularly bad halide choice), but for the most part, the product distribution, as determined by GC peak integrations, were very favourable for the desired amine substitution product. In each case, the arylamine was added under N<sub>2</sub> to the nitrite mixture which was then heated to ~ 65 °C for 10 minutes and stirred at room temperature for 2 hours with distilled acetonitrile (CH<sub>3</sub>CN) or water.

Unfortunately, when we tried the most promising conditions suggested by Table 2.1 on our aminothiazole substrate, very little to no substitution product was observed. The attempted reactions are summarized in Figure 2.1. Fortunately, one set of conditions did work very well as discussed in the next sections. The big X in Figure 2.1 indicates that none of these reactions worked.

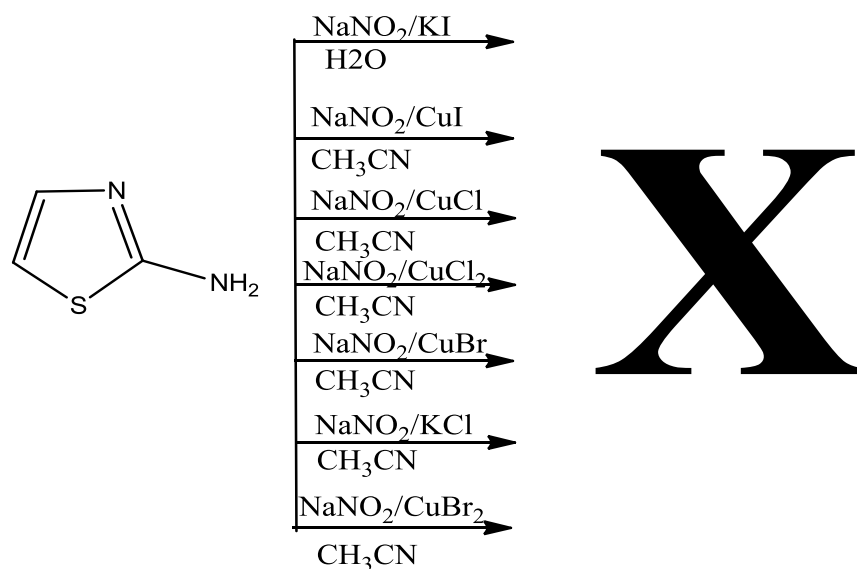


**Figure 2.1: Attempted Sandmeyer reactions on 2-amino-4-hexyl-1,3-thiazole**

**Table 2.1: Results of the Sandmeyer reaction on aniline substrate (Yields are reported as relative GC peak integrations of volatile products. Products were identified by their GC retention times (comparing with pure standards) and NMR spectroscopy on the reaction mixtures. Relative GC yields were verified by comparing to NMR peak integrations)**

NO <sub>2</sub> <sup>-</sup> Source	Ionic Salt	% Mono-halogenated Benzene	% of Starting material	% of Benzene	Total % of other products
NaNO <sub>2</sub>	KBr	76.40	21.30	0.00	2.30
	KI	69.40	30.10	0.00	0.50
	KCl	0.00	100.00	0.00	0.00
	CuI	87.90	10.00	2.00	0.10
	CuCl	98.70	1.00	0.30	0.00
	CuCl <sub>2</sub>	78.34	12.20	5.60	3.86
	CuBr <sub>2</sub>	68.90	14.40	12.30	4.40

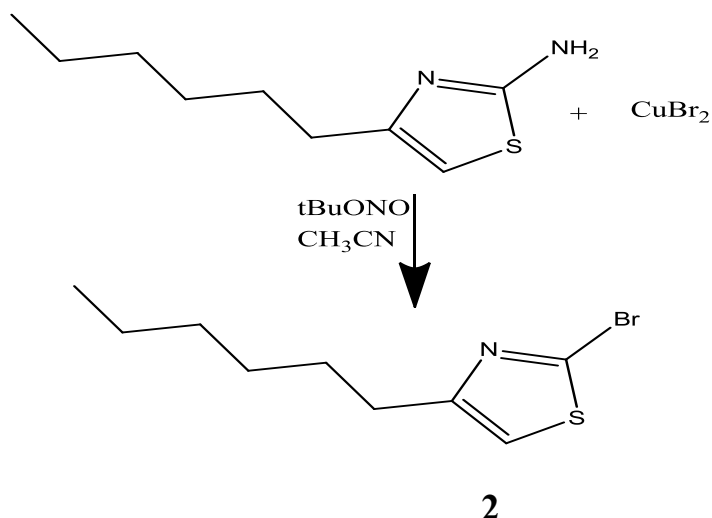
nBuONO	KBr	26.30	0.00	46.90	26.60
	KI	52.20	0.00	2.60	45.10
	KCl	0.00	2.40	78.50	19.20
	CuI	78.70	0.00	1.30	20.00
	CuCl	68.50	3.50	11.50	16.60
	CuCl <sub>2</sub>	80.50	4.00	8.70	6.90
	CuCl <sub>2</sub>	78.26	6.70	4.50	10.50
	CuBr <sub>2</sub>	72.80	7.40	6.70	13.10
	CuBr <sub>2</sub>	79.10	6.40	5.30	9.20
tBuONO	KBr	58.50	3.30	35.90	2.40
	KI	6.30	34.90	15.00	43.80
	KCl	14.00	34.40	5.40	46.00
	CuI	78.70	0.00	1.30	20.00
	CuCl	87.60	1.00	1.30	10.10
	CuCl <sub>2</sub>	86.90	1.30	3.20	8.0
	CuBr <sub>2</sub>	94.00	1.70	1.90	2.40
	CuBr <sub>2</sub>	89.20	1.25	2.39	7.25

### 2.2.3 Synthesis of 2-bromo-4-hexyl-1,3-thiazole

To deaminate 2-amino-4-hexyl-1,3-thiazole, we tried different conditions on this compound as described in Section 2.2.2 with the addition of copper (II) bromide as a source of salt, tert-butyl nitrite as a source of nitrite and acetonitrile as a solvent we successfully replaced bromine with the amine on the thiazole ring with a 90 % yield as shown in Scheme 2.7. Loss of NH<sub>2</sub> was verified by IR and MS which showed a characteristic 1:1 bromo peak as well as a

molecular ion consistent with the correct molar mass, leading to the M+1 peak, presumably due to protonation on the thiazole nitrogen.

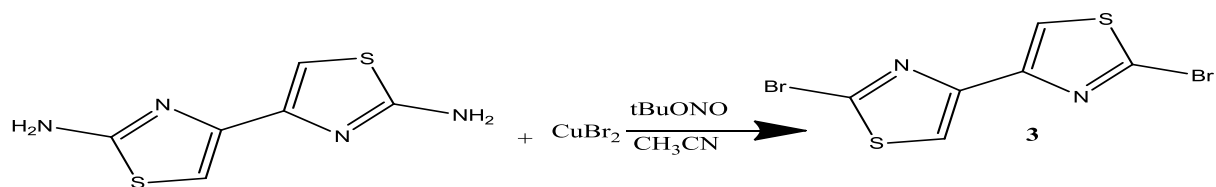
### Scheme 2.7: Synthesis of 2-bromo-4-hexyl-1,3-thiazole



### 2.2.4 Synthesis of 2,2'-diamino-4,4'-bithiazole

Starting from commercially available 2,3-butanedione and thiourea, 2,2'-diamino-4,4'-bithiazole was prepared by the literature route.<sup>46,47,48</sup> Using the optimal conditions outlined in Section 2.2.2, 2,2'-diamino-4,4'-bithiazole was substituted to give 2,2'-dibromo-4,4'-bithiazole as shown in Scheme 2.8. Characterization data (NMR, IR, and mass spectra) were as expected. This method was scaled up to provide sufficient amounts to do further reactions.

### Scheme 2.8: Deamination of 2,2'-diamino-4,4'-bithiazole



We successfully synthesized 2-bromo-4-hexyl-1,3-thiazole and 2,2'-dibromo-4,4'-bithiazole compounds and we found the best set of Sandmeyer conditions for thiazoles is the use of copper

(II) bromide as a source of salt, tert-butyl nitrite as a source of nitrite, and acetonitrile as a reaction solvent at 65 °C, yielding 1.05 g, 65 % of the product.

## 2.3 Experimental

### 2.3.1 General

1-Bromo-2-octanone and 2,2'-diamino-4,4'-bithiazole were synthesized by the literature routes.<sup>46, 47, 48, 49</sup> Nuclear magnetic resonance (NMR) spectra were obtained on a Varian Unity Innova 500 (11.74 T). Mass spectra were obtained on the Advion-Expression Compact Mass Spectrometer; nitrogen atoms tend to protonate in the instrument, leading to + 1 mass unit for each N atom in the molecule. Infra red spectra were collected on a Nicolet 380 FT-IR with a resolution of 1cm<sup>-1</sup>. Acetonitrile was dried over P<sub>2</sub>O<sub>5</sub> and distilled prior to use. CuBr<sub>2</sub> was dried by heating *in vacuo* and stored in a desiccator.

### 2.3.2 Preparation of 2-amino-4-hexyl-1,3-thiazole (1)

1-Bromo-2-octanone (4.27g, 20.6 mmol) and thiourea (1.57 g, 20.6 mmol) were weighed into a 500 mL round bottom flask. The mixture was dissolved in 50 mL of ethanol equipped with a stir bar. The mixture was refluxed for 3 hours under nitrogen gas. The resulting solution was added to 100 mL of water and neutralized to pH 9 with sodium carbonate. The product was extracted with diethyl ether and dried with magnesium sulfate, rotavapped, and then vacuum distilled to give a light yellow oil (3.41g, 90 %). <sup>1</sup>H NMR (500 MHz, CDCl<sub>3</sub>, δ (ppm), *J*(Hz)): δ 0.89 (3H, t, *J* = 7.0 Hz), 1.30 (4H, m), 1.52 (2H, m), 2.08 (2H, m), 2.50 (2H, t, *J* = 7.0 Hz), 5.95 (s, br), 5.97 (s, shoulder)) (note: the broad NH<sub>2</sub> peak overlaps the aromatic C-H, causing the latter to appear as a shoulder on the NH<sub>2</sub> peak). <sup>13</sup>C NMR (126 MHz, CDCl<sub>3</sub>, δ (ppm)): 13.95, 14.36, 22.37, 22.58, 26.05, 31.09, 102.07, 153.66, 167.15. IR (nujol mull): 3286 (s, br), 3116 (s, br), 1619 (s), 1524 (s), 1107 (w) cm<sup>-1</sup>. Mass spec. calc. for C<sub>9</sub>H<sub>15</sub>N<sub>2</sub>S 183, found 185 (100 %,



M+2), 183 (2 %, M).

### 2.3.3 Preparation of 2-bromo-4-hexyl-1,3-thiazole (2)

2-Bromo-5-hexyl-1,3-thiazole was synthesized from copper (II) bromide (3.98 g, 17.8 mmol), *tert*-butyl nitrite (1.84 g, 17.8 mmol) and 30 mL of acetonitrile as a solvent, which was weighed into a 3-necked round bottom flask with gas outlet, joint, and a thermometer equipped with a stir bar. The mixture was stirred under nitrogen gas and refluxed to approximately 65 °C. The 2-amino-5-hexyl-1,3-thiazole (3.3 g, 17.8 mmol) in 3 mL of acetonitrile was slowly added to the reaction mixture over a period of 5 minutes. During this addition the reaction solution turned black as nitrogen was evolved. The mixture was left to stir at this temperature for 10 minutes, then cooled to room temperature, and stirred for 2 hours. The product mixture was poured into 100 mL of 20 % aqueous hydrochloric acid, extracted into 2\*100 mL of ether, rewash with 100 mL of 20 % aqueous hydrochloric acid. The ether containing product was dried with magnesium sulfate and the ether was removed under reduced pressure. Purification by column chromatography (silica gel, 80:20 hexane: ether) yielded (3.28 g, 82.5%) of the product. <sup>1</sup>H NMR (500 MHz, CDCl<sub>3</sub>, δ (ppm), *J*(Hz)): δ 0.89 (3H, t, *J* = 7.0 Hz), 1.18-1.35 (4H, m), 1.48 (2H, tt, *J* = 10.1, 7.0 Hz), 2.69 (2H, t, *J* = 10.1 Hz), 7.68 (1H, s). IR (nujol mull): 1685 (s), 1653(w), 1424 (m), 1373 (m), 1242 (s), 1047 (s), 790 (w) cm<sup>-1</sup>. Mass spec. calc. for C<sub>9</sub>H<sub>14</sub>BrNS: 247, 249. Found 247, 249.9 (100 % M+1)<sup>+</sup>.

### 2.3.4 Synthesis of 2,2'-dibromo-4,4'-bithiazole (3)

Copper (II) bromide (2.25g, 10 mmol), *tert*-butyl nitrite (1.03 g, 10 mmol) and 40 mL of acetonitrile were weighed into a 3-necked round bottom flask fitted with a gas outlet, a thermometer, and a stir bar. The mixture was stirred under nitrogen gas and refluxed at approximately 65 °C. 2,2'-Diamino-4,4'-bithiazole (1g, 5.0 mmol), as a solid, was slowly added

to the reaction mixture over a period of 5 minutes. During this addition the reaction solution turned completely black as nitrogen was evolved. The mixture was left to stir at this temperature for 10 minutes then allowed to reach room temperature and stirred for 2 hours. The product mixture was poured into 100 mL of 20 % aqueous hydrochloric acid, extracted into 2\*100 mL of ether, rewashd with 100 mL of 20 % aqueous hydrochloric acid, dried over magnesium sulfate, and then rotavapped to remove the ether. The yield for the reaction was 1.05 g, 65 % .  $^1\text{H}$  NMR (500 MHz,  $\text{CDCl}_3$ ,  $\delta$  (ppm)): 8.16.  $^{13}\text{C}$  {H} NMR (126 MHz,  $\text{CDCl}_3$ )  $\delta$  (ppm): 111.45, 135.61, 145.77. IR (nujol mull): 2734 (w), 1720 (m), 1000 (s), 730 (s), 750 (m)  $\text{cm}^{-1}$ . Mass spec. calc. for  $\text{C}_6\text{H}_2\text{N}_2\text{S}_2\text{Br}_2$  326.80, found 325.98 (100 %,  $\text{M}^+$ ).

## Chapter 3-Synthesis of mixed oligomers

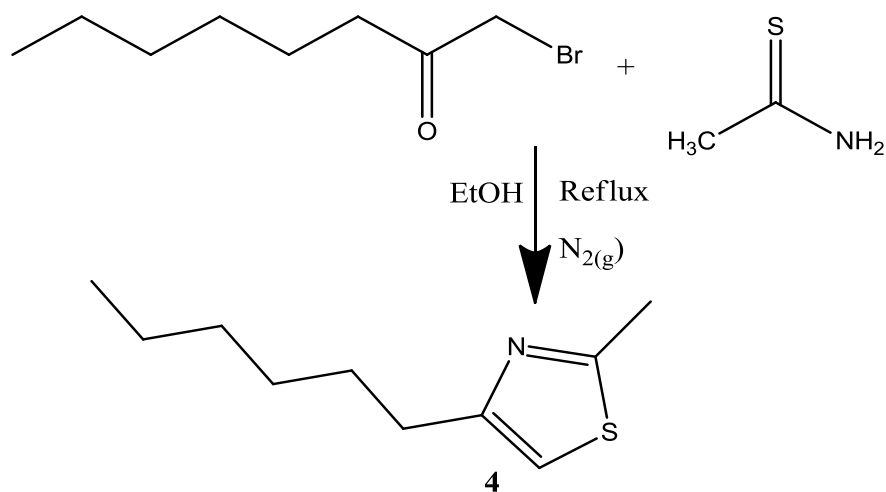
Organic semiconductors are used as an alternative to inorganic semiconductors in areas as diverse as organic photovoltaic devices, organic light-emitting diodes (OLEDs), and organic field-effect transistors (OFETs) as described in section 1.1.2. Specifically, this chapter looks at developing synthetic methods to generate new oligomeric semiconductors. Parameters such as the HOMO-LUMO gap, how the electrons are packed, how molecules adhere to the substrate, and electron mobility can be affected by changing the heteroatom on the ring. Specifically, we wish to generate a series of quaterthiophene analogues where at least one of the thiophene rings is replaced by another ring type, *e.g.* thiazole, furan, or pyrrole. Each of these substitute rings should be more electron withdrawing than the thiophene it has replaced.

### 3.1 Ring systems used in this study

In order to tune the performance of these oligomers, we seek to incorporate other rings such as thiazole, furan, and pyrrole. Such replacements have been reported to be effective in reducing the steric interaction due to the absence of one hydrogen atom. Stability of the molecule may also be increased upon substitution.<sup>50</sup> Mixed oligomers can be prepared piece-by-piece through mixing and matching ring-containing organic synthons. Synthons used in this study are discussed in this section. For traditional Stille, Suzuki, and Kumada coupling reactions, brominated rings are required. NBS in DMF can be used when brominating heterocyclic rings.<sup>51</sup> As previously mentioned, the ring-closing synthesis of the 1,3-thiazole ring allows some flexibility in the resulting ring substituents, as well as in the location of the substituents relative to ring-ring connectivity. In Chapter 2, we reported the synthesis of 2-amino-4-hexyl-1,3-thiazole, which, when the amine is converted to a halogen, can be used as one of our synthons.

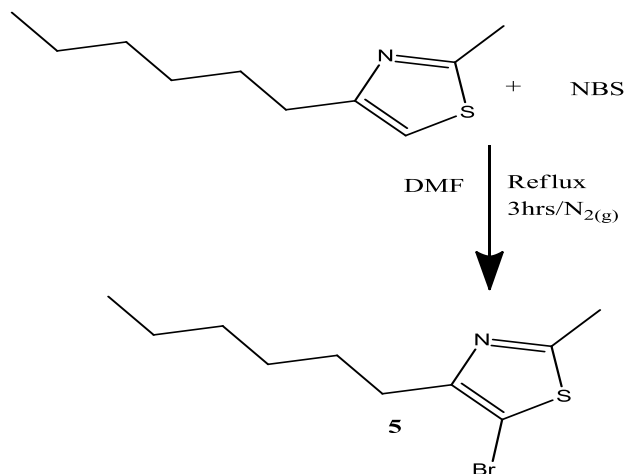
Another synthon is 5-bromo-4-hexyl-2-methyl-1,3-thiazole. This compound is generated in two steps. The first is the condensation reaction between 1-bromooctanone and thioacetamide (4.49 g, 80 %), Scheme 3.1 to generate the protonated ring **4**.

**Scheme 3.1: Synthesis of 4-hexyl-2-methyl-1,3-thiazole**



Compound **4** is then brominated with NBS. The bromine selectively attaches to the ring to form **5** (3.79 g, 90 %), Scheme 3.2.

**Scheme 3.2: Synthesis of 5-bromo-4-hexyl-2-methyl-1,3-thiazole**



Another ring we used is furan. Bromofuran (**6**) was prepared immediately before use according to the literature procedure.<sup>52</sup> A reaction temperature of 35 °C was maintained during the addition

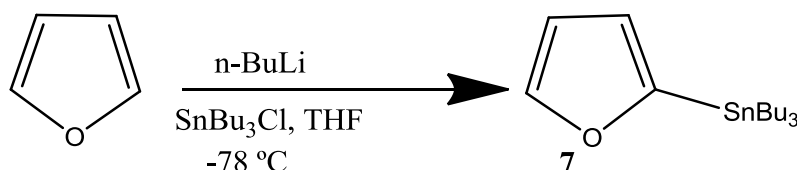
of NBS to the DMF solvent, after which the reaction was slowly heated to 120 °C. (12.85 g, 78 %), Scheme 3.3.

### Scheme 3.3: Synthesis of Bromofuran



Alternatively, stannylated furan can be used as a furan synthon. 2-(Tributyltin)-furan was synthesized from furan by lithiation using *n*-butyllithium followed immediately by stannylation with tributyltin chloride at -78 °C to **7**. Excess tin was removed by dissolving **7** in ether and washing with 1M sodium hydroxide, (13.75 g, 95 %) Scheme 3.4.<sup>53</sup>

### Scheme 3.4 Synthesis of 2-(tributyltin)-furan



Also, attaching *N*-pyrrole to the bithiazole moiety, we employed the Clauson-Kaas pyrrole synthesis, whereby a pyrrole oligomer is synthesized by the condensation of 2,5-dimethoxytetrahydrofuran with a primary amine.<sup>54</sup>

## 3.2 Coupling methods

In order to connect rings together, we used several coupling methods including the Kumada,<sup>55,56</sup> Stille,<sup>57</sup> and Suzuki<sup>58</sup> reactions.

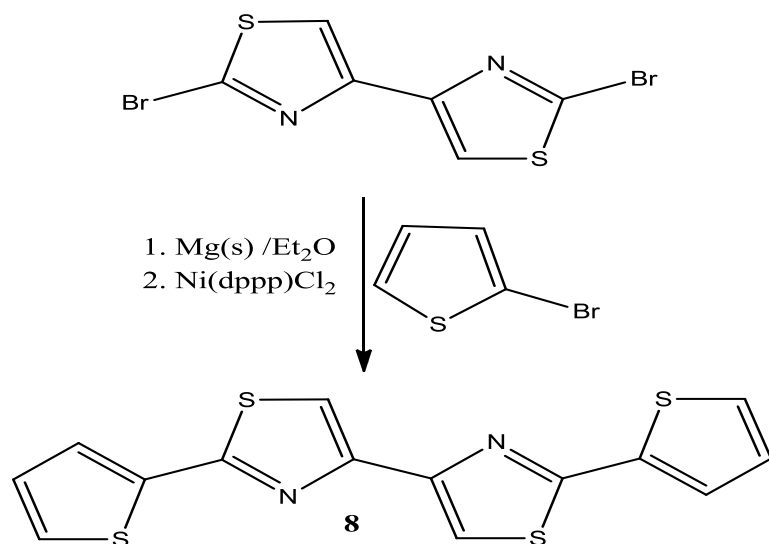
### 3.2.1 Grignard-type synthesis of oligomers

Kumada coupling was the first Ni-catalyzed cross-coupling reaction. It involves an organo

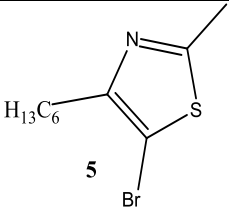
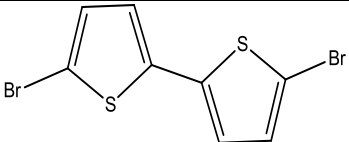
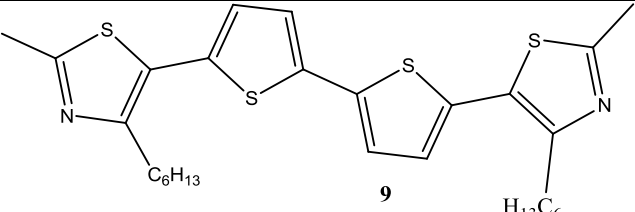
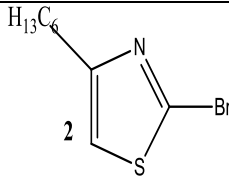
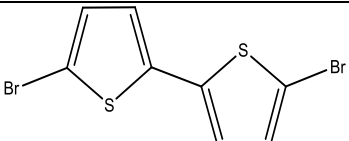
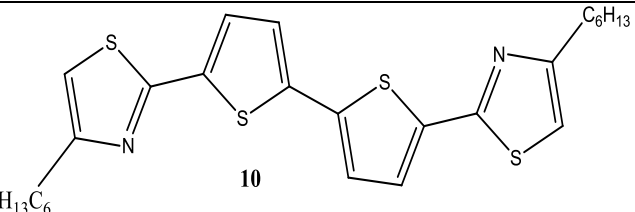
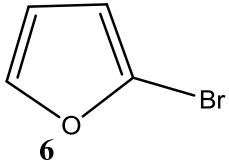
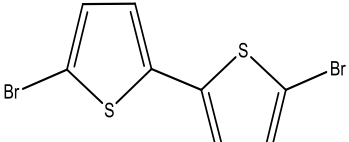
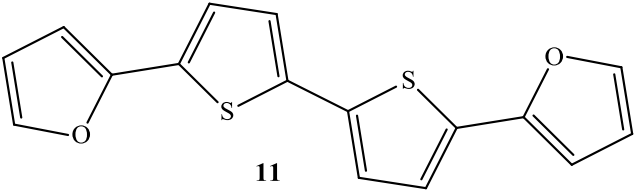
magnesium halide and an organo halide in the presence of a nickel catalyst, forming the coupled product (C-C bond). The advantage of this reaction is the direct coupling of Grignard reagents, which avoids additional reaction steps such as the conversion of Grignard reagents to zinc compounds for a Negishi<sup>59</sup> coupling reaction.

Compounds 5,5'-bis(5-(4-hexyl-2-methyl)-thiazolyl)-2,2'-bithiophene (**9**) and 5,5'-bis(2-furanyl)-5,5'-bithiophene (**11**) were successfully prepared by the Grignard reaction. Attempts to generate the proposed tetracyclic oligomers 2,2'-bis(2-thienyl)-4,4'-bithiazole (**8**) and 5,5'-bis(2-(4-hexyl)-thiazolyl)-2,2'-bithiophene (**10**) were also attempted via the Kumada method but without success. Converting bromothiophene to the organomagnesium agent was chosen because there has been no report in the literature of both ends of an aryl halide being metallated. 2,2'-Dibromo-4,4'-bithiazole was coupled with bromomagnesiumthiophene in the presence of a nickel catalyst (Ni(dppp)Cl<sub>2</sub>) where dppp is 1,3-bis(diphenylphosphino)propane, and ether as solvent to yield the coupled compound 2,2'-bis(2-thienyl)-4,4'-bithiazole (**8**), (0.32 g, 65 %), (Scheme 3.5). For experimental details on compounds **8** and **10**, see appendix 1 and 2. Table 3.1 summarizes the Kumada routes to the synthesis of the compounds 5,5'-bis(5-(4-hexyl-2-methyl)-thiazolyl)-2,2'-bithiophene (**9**) and 5,5'-bis(2-furanyl)-5,5'-bithiophene (**11**). The Grignard syntheses summarized in Table 3.1 were all performed as for compound **8**. As indicated above compound **8** and **10** were not successfully synthesized.

**Scheme 3.5: Synthesis of 2,2'-bis(2-thienyl)-4,4'-bithiazole**



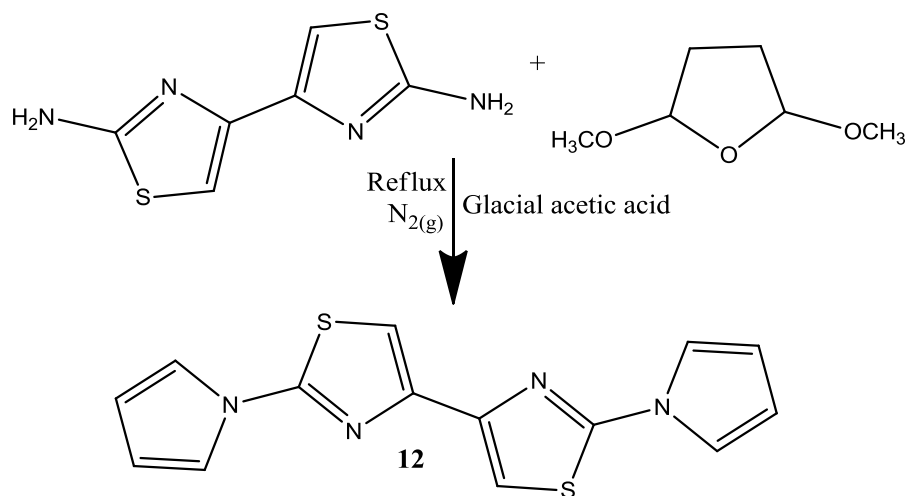
**Table 3.1 The Kumada synthesis of compounds 9, 10, and 11**

Halogenated compounds	organohalide	Oligomeric Product
 <p><b>5</b></p>	 <p>5,5'-dibromo-2,2'-bithiophene</p>	 <p><b>9</b></p>
 <p><b>2</b></p>	 <p>5,5'-dibromo-2,2'-bithiophene</p>	 <p><b>10</b></p>
 <p><b>6</b></p>	 <p>5,5'-dibromo-2,2'-bithiophene</p>	 <p><b>11</b></p>

### 3.2.2 Synthesis of 2,2'-bis(*N*-pyrrolyl)-4,4'-bithiazole (12)

Compound **12** was synthesized via the Clauson-Kaas pyrrole synthesis as shown in Scheme 3.6. 2,2'-Diamino-4,4'-bithiazole was reacted with 2,5-dimethoxytetrahydrofuran and refluxed in glacial acetic acid, (50 ml) as a reaction solvent for 48 hours under nitrogen atmosphere. After the 48 hours, the glacial acetic acid was evaporated off via a rotary evaporator. The remaining crude product was dissolved in dichloromethane, washed with sodium hydroxide followed by sodium bicarbonate. The resulting product was purified on a silica gel column eluting with dichloromethane and hexane, 2:1, with a yield of 0.45 g, 52 %.

#### Scheme 3.6: Synthesis of 2,2'-bis(*N*-pyrrolyl)-4,4'-bithiazole (12)



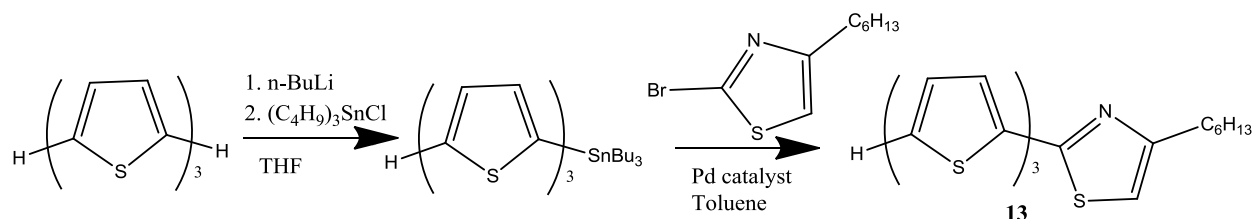
### 3.2.3 Attempted synthesis of 5-(4-hexyl-1,3-thiazolyl)-2,2':5',2'-terthiophene (13)

Compound **13** was synthesized (attempted) via Stille coupling as shown in Scheme 3.7. The Stille coupling reaction is a versatile C-C bond-forming reaction between organostannanes and halides, with very few limitations on the R-groups. The toxicity of tin compounds is the main drawback of this coupling reaction. In addition, their low polarity makes them poorly soluble in solvents such as water. Lithiation followed immediately by stannylation of 2,2':5',2''-



terthiophene at  $-78\text{ }^{\circ}\text{C}$  gave 2-(tributyltin)-2,2':5,2''-terthiophene, which is then reacted with 2-bromo-4-hexyl-1,3-thiazole in the presence of a palladium catalyst to yield (7.5 g, 97 %) of product (Scheme 3.7). For experimental details see appendix 3.

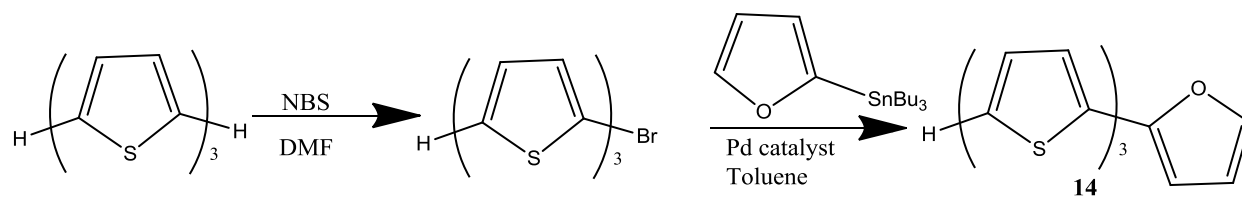
**Scheme 3.7: Synthesis of 5-(4-hexyl-1,3-thiazolyl)-2,2':5,2''-terthiophene (13)**



**3.2.4 Attempted synthesis by Stille coupling of 5-(2-furanyl)-2,2':5,2''-terthiophene (14)**

Compound 14 was attempted synthesis from 5-bromo-2,2':5,2''-terthiophene and 2-(tributylstannyl)-furan via Stille coupling. The bromination of 2,2':5,2''-terthiophene was done at  $-20\text{ }^{\circ}\text{C}$  because the solubility of 5-bromo-2,2':5,2''-terthiophene is low at that temperature, such that it precipitates before dibromination can occur.<sup>38</sup> Reaction between 5-bromo-2,2':5,2''-terthiophene and 2-(tributylstannyl)furan in the presence of tetrakis(triphenylphosphine)Pd(0) as a catalyst yielding (2.3 g, 70.34 %) of product (Scheme 3.8). For experimental details see appendix 4.

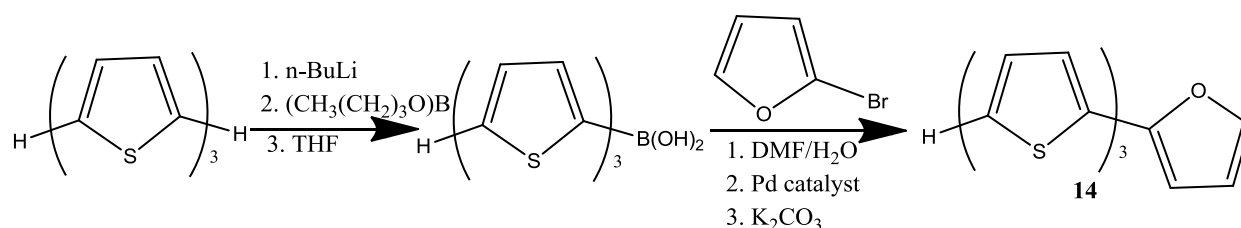
**Scheme 3.8: Stille coupling of 5-(2-furanyl)-2,2':5,2''-terthiophene (14)**



### 3.2.5 Suzuki coupling of 5-(2-furanyl)-2,2':5,2''-terthiophene (14)

Compound **14** was synthesized via Suzuki coupling of arylboronic acid, 2,2':5,2''-terthiophene-5-boronic acid and bromofuran in the presence of a palladium catalyst. Borylation was achieved by reacting terthiophene with butyllithium at  $-35\text{ }^{\circ}\text{C}$ , followed by addition of tributylborate at  $-65\text{ }^{\circ}\text{C}$ . The resulting 2,2':5,2''-terthiophene-5-boronic acid and bromofuran were coupled using bis(triphenylphosphine)palladium chloride as the catalyst and potassium carbonate as the base. The details of the reaction are shown in scheme 3.9.

**Scheme 3.9: Suzuki coupling of 5-(2-furanyl)-2,2':5,2''-terthiophene**



## 3.3 Results and discussion

We determined the results of the above reactions through characterization of the reaction products using NMR ( $^1\text{H}$  and  $^{13}\text{C}$ ) and IR spectroscopy, and low resolution mass spectrometry. For compounds **9**, **11**, **12**, and **14**, we have evidence that these reactions worked. The results are shown in the proton and carbon NMR as well as in the mass spectrometry analysis. In the NMR characterization it was observed that all the starting material peaks were not seen in the spectra after the coupling reaction. In compound **11**, the product has very low solubility in hexane, toluene, ether and water, making purification and  $^{13}\text{C}$  NMR difficult to obtain. Even minute amounts of the much more soluble starting material (and perhaps by-products) leads to spurious peaks in the NMR that obscure the product peaks. The high-solubility impurities will have much more intense signals, so running more scans was also not feasible. However, the mass spectra

clearly shows the peak with the correct product mass, as does the  $^1\text{H}$  NMR, which, when compared with the simulated spectrum, contains peaks consistent with the product (among other things, such as the dibromobithiophene starting material). As with the  $^{13}\text{C}$  NMR, there is overlap of peaks and a coincidental overlap with the residual chloroform peak, preventing accurate coupling constants and integration values. The calculated molecular mass was 300.0, which corresponds nicely with the mass spectrum peak (also at 300.0).

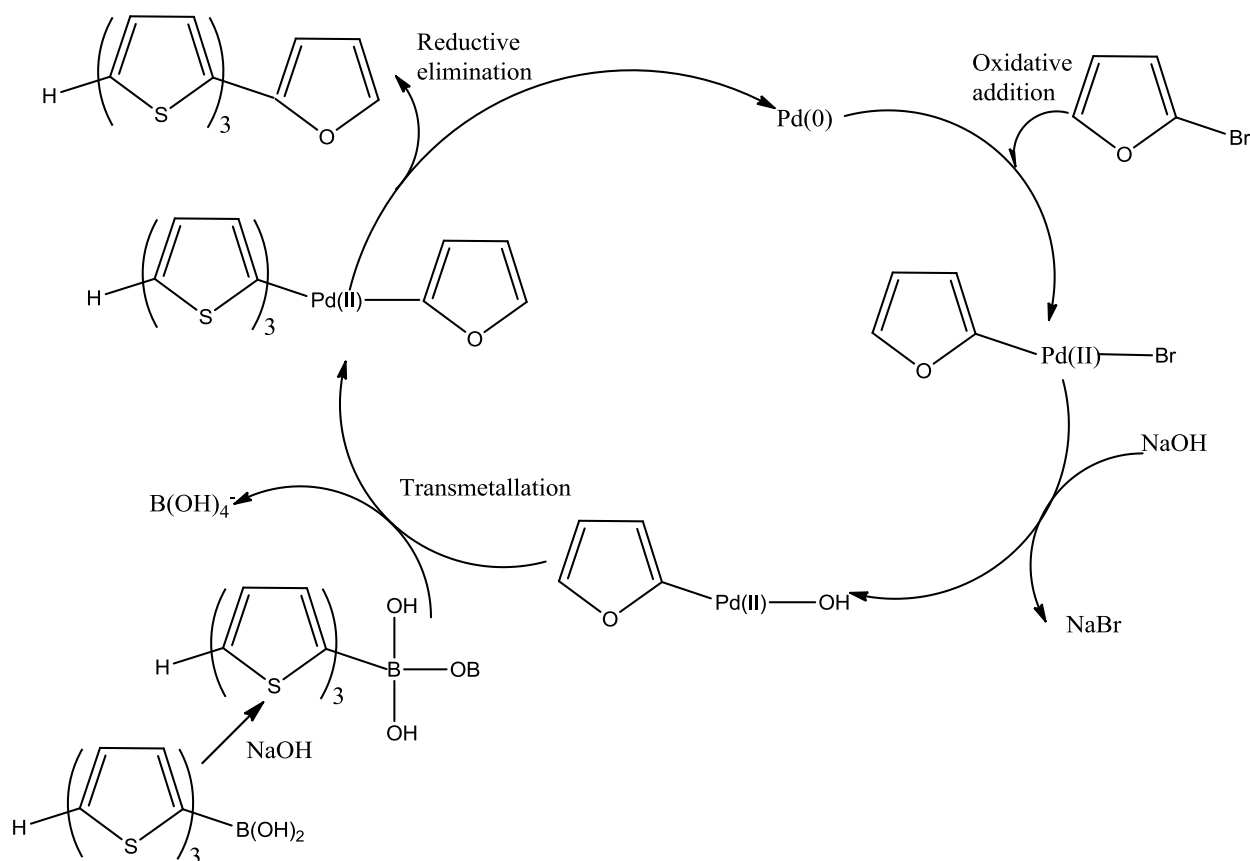
In compound **12**, the calculated molecular mass was 298.4 and our spectra showed a molecular mass of 299.1. The  $M+1$  peak is reasonable because in the mass spectra there could be a proton adding or we isolated the protonated product (presumably protonated during the workup), which would not be surprising given the existence of basic nitrogens in the compound.

For compound **9**, the calculated molecular mass was 528, while the MS base peak is located at 264.0. This peak is consistent with exactly half of the molecule, *i.e.* the fragment hexyl-methyl-thiazole-thiophene (Hx-Me)-Tz-T. Because of the synthetic route, there is no logical way to form this fragment from unreacted starting materials, we therefore propose that the reaction was successful, but that the molecule was subsequently cleaved in the spectrometer (perhaps because it is thermally unstable, perhaps because the intact molecular ion is not volatile enough, etc.). It is also possible that we are seeing a doubly-ionized species  $M^{2+}$ , but we consider this less likely in light of the fact that we see no evidence in our other compounds of an  $M^{2+}$  peak. This results is only evidence, albeit not definitive proof that the initial coupling reaction took place and **9** was successfully synthesized.

Lastly, for compound **14**, the calculated molecular mass was 314 but in our spectra we have 249, which is the mass of a terthiophene fragment. We proposed that the oxidative addition

part of the mechanism worked, that is the carbon-boron bond was added across the palladium in the catalyst, but the subsequent reductive elimination of the product (or perhaps the second oxidative addition of the bromofuran) did not occur as shown in Scheme 3.10. The  $^{13}\text{C}$  NMR spectrum is consistent with terthiophene as the main isolated product.

**Scheme 3.10: Mechanism for Suzuki coupling reaction for compound 14**



On the other hand, in compounds labelled **8**, **10**, **13**, and **15**, we believed the reaction was partly completed, we are less confident in their characterization because we have difficulties purifying them. This is because longer oligomers are insoluble and do not pass through chromatography columns very well. We conclude that there will be a need to develop methods to

purify these oligomers. Also these oligomers could polymerize as the Stille reaction has the potential to be developed as a new polymerization tool.<sup>60, 61</sup>

## 3.4. Experimental

### 3.4.1 General synthetic and instrumental details

Unless otherwise indicated, all reactions were conducted under an inert nitrogen atmosphere following standard Schlenk techniques using a double manifold vacuum-line with a Savant VLP 200 series rotary vacuum pump. Nuclear magnetic resonance spectra were obtained using a Varian Unity Inova 500 spectrometer at the Lakehead University Instrument Laboratory. All spectra were recorded at room temperature and chemical shifts were internally referenced to tetramethylsilane (TMS) and are reported in parts per million (ppm). Mass spectra were obtained on the Advion-Expression Compact Mass Spectrometer; nitrogen atoms tend to protonate in the instrument, leading to +1 mass unit for each N atom in the molecule. Infrared spectra were collected on a Nicolet 380 FT-IR with a resolution of  $1\text{ cm}^{-1}$ . Glassware used for Grignard reactions was oven dried, evacuated, and purged with  $\text{N}_2$  (g) several times and allowed to cool to room temperature. 2,2'-Bithiophene,<sup>54,55</sup> 5,5-dibromo-2,2-bithiophene,<sup>51</sup> 2-bromofuran,<sup>52</sup> 2,2':5,2''-terthiophene,<sup>53,54</sup> 5-bromo-2,2':5',2''-terthiophene,<sup>51</sup> 2-(tributyltin)-2,2':5',2''-terthiophene,<sup>62</sup> 2-(tributyltin)-furan,<sup>53,64</sup> and 2,2':5,2''-terthiophene-5-boronic acid<sup>63</sup> were synthesized according to the literature route. All solvents were dried and degassed under nitrogen atmosphere. All other reagents were obtained commercially from Millipore-Sigma or Fisher Scientific and used as received.

### 3.4.2 Preparation of 5,5'-bis(4-hexyl-2-methyl-thiazolyl)-2,2'-bithiophene (9)

#### 3.4.2.1 Preparation of 4-hexyl-2-methyl-1,3-thiazole (4)

1-Bromo-2-octanone (6.40 g, 30.9 mmol) was weighed into 75 mL of ethanol in a 500 mL round bottom flask equipped with a stir bar and a reflux condenser. Thioacetamide (2.33 g, 31.0 mmol) was added. The resulting mixture was refluxed under nitrogen gas for 3 hours and was allowed to cool. After the 3 hour period, the solution was poured into 100 mL of distilled water and was neutralized to a pH of 9 using saturated sodium carbonate. The organic product was extracted with ether and dried with  $\text{MgSO}_4$ . The solvent was removed via rotary evaporation. The resulting product was further purified via fractional distillation to obtain a yellowish-brown oil (4.49 g, 80 %).  $^{13}\text{C}$  NMR (126 MHz,  $\text{CDCl}_3$ )  $\delta$  (ppm): 14.30, 18.46, 22.22, 23.44, 28.53, 31.31, 43.34, 111.81, 157.15, 165.01. IR (neat): 1720 (s), 1570 (m), 2809 (s), 758 (w)  $\text{cm}^{-1}$ . Mass spec. calc. for  $\text{C}_{10}\text{H}_{17}\text{NS}$ : 183; found: 184 (100%,  $\text{M}+1$ ).

#### 3.4.2.2 Preparation of 5-bromo-4-hexyl-2-methyl-1,3-thiazole (5)

A 1.5 : 1 molar ratio of *N*-bromosuccinimide (NBS): compound 4 was used. Compound 4 (3.00 g, 16.19 mmol) was weighed and dissolved into 70 mL of dimethylformamide (DMF) equipped with a stir bar. To the stirred mixture, NBS (4.32 g, 24.27 mmol) was added portionwise over the course of 2 hours. The mixture was stirred and refluxed for approximately for 3 hours under nitrogen gas. The resulting mixture was poured into 100 mL of distilled water and the product extracted into dichloromethane. The organic fractions were dried over  $\text{MgSO}_4$ . The solvent was removed via rotary evaporation. The product was further purified by vacuum distillation at 70-75 °C at  $10^{-1}$  Torr (3.79 g, 90 %).  $^{13}\text{C}$  NMR (126 MHz,  $\text{CDCl}_3$ )  $\delta$  (ppm): 13.68, 16.09, 19.27, 22.74, 26.50, 30.07, 36.62, 120.55, 142.91, 147.53. IR (nujol mull): 1783 (s), 1727 (s), 1470 (m), 1191 (s), 1041 (m), 1007 (w)  $\text{cm}^{-1}$ . Mass spec. calc. for  $\text{C}_{10}\text{H}_{16}\text{BrNS}$ : 261, 263.

Found: 261.9, 263.9 (100%, M+1), 184.0 (80 %, C<sub>10</sub>H<sub>18</sub>NS<sup>+</sup>).

### 3.4.2.3 Preparation of 5,5'-bis(4-hexyl-2-methyl-thiazolyl)-2,2'-bithiophene (9)

A 2:1 molar ratio of compound **5** and 5,5'-dibromo-2,2'-bithiophene was used. Compound **5** (1.64 g, 6.17 mmol) was weighed into 20 mL of dried ether and the resulting solution added dropwise to magnesium turnings (0.54 g, 21.00 mmol) in 10 mL of dried ether at 0 °C. A pellet of iodine was added to initiate the Grignard reaction. The resulting mixture was stirred at room temperature for 3 hours under nitrogen atmosphere. A second mixture was prepared containing Ni(dppp)Cl<sub>2</sub> (0.1 g, 0.18 mmol) and 5,5'-dibromo-2,2'-bithiophene (1 g, 3.09 mmol) in 20 mL of ether. Both mixtures were cooled to 0 °C. The Grignard reagent solution was cannulated into the bithiophene mixture and left to stir overnight under N<sub>2</sub> (g). After this time, the mixture was added to 60 mL of NH<sub>4</sub>Cl, followed by extraction into ether. The organic fractions were dried over MgSO<sub>4</sub>. The ether solvent was removed via rotary evaporation to obtain a yellowish-brown solid (0.9 g, 42 %). <sup>1</sup>H NMR (500 MHz, CDCl<sub>3</sub>) δ (ppm): 0.89 (t, 3H, *J* = 7 Hz), 1.19 (m, 6H), 1.3 (m), 1.30 (m, 6H), 2.21 (m, 4H), 2.64 (m, 4H), 2.92 (m, 4H), 6.82 (d, 2H, *J* = 3.5), 6.94 (d, 2H, *J* = 3.5), 7.67 (d, 2H, *J* = 7.7 Hz), 7.42 (d, 2H, *J* = 7.7 Hz). <sup>13</sup>C NMR (126 MHz, CDCl<sub>3</sub>) δ (ppm) : 11.34, 14.03, 22.43, 25.35, 28.95, 29.49, 31.74, 124.17, 128.91, 130.79, 131.91, 132.13, 137.79, 163.36. IR (nujol mull): 3073 (m), 1705 (s), 1416 (s), 1376 (s), 1172 (m), 847 (m), 778(s) cm<sup>-1</sup>. Mass spec. calc. for C<sub>28</sub>H<sub>36</sub>N<sub>2</sub>S<sub>4</sub> is 528; found 264 (100 %, C<sub>14</sub>H<sub>18</sub>NS<sub>2</sub><sup>+</sup>).

### 3.4.3 Preparation of 5,5'-bis(2-furanyl)-2,2'-bithiophene (11)

A 2:1 molar ratio of 2-bromofuran and 5,5'-dibromo-2,2'-bithiophene was used. 2-Bromofuran (2 g, 13.6 mmol, 2.0 eqv) was weighed into 20 mL of dried THF and the resulting solution added dropwise to magnesium turnings (0.54 g, 22 mmol) in 10 mL of dried THF at 0 °C. A pellet of iodine was added to initiate the Grignard reaction. The mixture was kept at reflux

temperature throughout the addition. The resulting mixture was stirred at room temperature for 3 hours under a nitrogen atmosphere. A second mixture was prepared containing Ni(dppp)Cl<sub>2</sub> (0.1 g, 0.18 mmol) and 5,5'-dibromo-2,2'-bithiophene (0.65 g, 2 mmol) in 20 mL of THF. Both mixtures were cooled to 0 °C. The Grignard reagent solution was cannulated into the bithiophene mixture and left to stir overnight under N<sub>2</sub> (g). After this time, the mixture was added to 60 mL of NH<sub>4</sub>Cl, followed by extraction into THF. The organic fractions were dried over MgSO<sub>4</sub>. The THF solvent was removed via rotary evaporation to obtain a yellowish-brown solid, which was subsequently purified by column chromatography (silica gel) using a solvent mixture of ethyl acetate and hexane. (1.6 g, 84 %). <sup>1</sup>H NMR (500 MHz, CDCl<sub>3</sub>) δ (ppm): 6.30 (m, 1H), 7.22 (m, overlap with CHCl<sub>3</sub>) 7.48 (d, 1H, *J* = 8.8 Hz), 7.62 (m, 2H, two overlapping peaks). <sup>13</sup>C NMR (126 MHz, CDCl<sub>3</sub>) δ (ppm): 111.59, 112.55, 124.22, 128.71, 132.83, 137.85, 144.39, 158.1. Mass spec. calc. for C<sub>16</sub> H<sub>10</sub> O<sub>2</sub> S<sub>2</sub> is 298, found 300 (100 % M+2)<sup>+</sup>.

#### 3.4.4 Preparation of 2,2'-bis(*N*-pyrrolyl)-4,4'-bithiazole (12)

2,2'-Bis(*N*-pyrrolyl)-4,4'-bithiazole was synthesized by the Clauson-Kaas condensation of 2,5-dialkoxytetrahydrofuran and a primary amine in the presence of an acid catalyst. The amine, 2,2-diamino-4,4'-bithiazole (0.58 g, 2.93 mmol) was added to 2,5-dimethoxytetrahydrofuran (1.1 mL) and refluxed in glacial acetic acid (50 mL). The mixture was refluxed for 48 hours under nitrogen gas. After the 48 hours, the glacial acetic acid was evaporated off with a rotary evaporator. The remaining crude product was dissolved in dichloromethane and washed with sodium hydroxide followed by sodium bicarbonate. The dichloromethane was evaporated off. The product was purified on silica gel with dichloromethane and hexane to give a yellowish-green powder with a yield of 0.45 g, 52 %. <sup>1</sup>H NMR (500MHz, CDCl<sub>3</sub>, δ (ppm): 6.51 (t, *J* = 2 Hz, 4H), 7.41 (t, 4H), 7.45 (s, 2H). <sup>13</sup>C NMR (126 MHz CDCl<sub>3</sub>, δ (ppm): 109.91, 112.10,



119.67, 147.36, 160.97. IR (nujol mull): 3116 (m), 1652 (m), 1472 (s), 1343 (s), 1327 (s), 1311 (w), 1109 (m), 1058 (m), 902 (m), 867 (m), 756 (s), 689 (m)  $\text{cm}^{-1}$ . Mass spec. calc. for  $\text{C}_{14}\text{H}_{10}\text{N}_4\text{S}_2$ : 298.4, found 299.1 ( $\text{M}+1$ )<sup>+</sup>.

### 3.4.5 Suzuki coupling of 5-(2-furanyl)-2,2':5,2''-terthiophene (14)

2,2':5,2''-Terthiophene-5-boronic acid (0.29 g, 1 mmol) under nitrogen gas was weighed into water/DMF (1 mL / 3 mL) in a three necked round bottom flask. Bromofuran (0.25 g, 1.7 mmol) was weighed and added to the flask. Bis(triphenylphosphine) palladium (II) dichloride,  $\text{PdCl}_2(\text{PPh}_3)_2$  (0.1 g, 0.02 mmol), as well as potassium carbonate (0.35 g, 2.5 eqv.) was added to the flask. The resulting mixture was heated to reflux under  $\text{N}_2$  (g) for 24 hours. After this time, the mixture was cooled to room temperature followed by the addition of 20 mL of water. The suspension obtained was extracted with ether (30 mL \*3) and the organic layer was washed with 100 mL of water and dried over anhydrous magnesium sulfate and the ether solvent was removed via rotary evaporation. The remaining crude product was purified by a silica gel column of hexane / ethyl acetate to give a shiny yellow solid (0.28 g, 89 %).  $^1\text{H}$  NMR (500 MHz,  $\text{CDCl}_3$ )  $\delta$  (ppm): 7.81 (dd, 1H,  $J = 1.90, 0.95$  Hz), 7.72 (d, 1H,  $J = 8.8$  Hz), 7.46 (d, H), 7.42 (dd, H), 7.33 (dd, H), 7.26 – 7.14 (m, H,  $J = 8.6, 1.2$  Hz), 7.09 (d,  $J = 0.5$  Hz, 1H), 6.97 (dd, 1H,  $J = 8.5, 4.9$  Hz), 6.56 (dd, 1H,  $J = 3.2, 0.8$  Hz, ), 6.51 – 6.43 (m, 1H,  $J = 3.2, 1.8$  Hz).  $^{13}\text{C}$  NMR (126 MHz,  $\text{CDCl}_3$ )  $\delta$  (ppm): 105.06, 111.23, 111.48, 123.56, 123.67, 124.29, 124.37, 124.46, 127.87, 128.99, 136.17, 136.34, 136.99, 137.10, 141.72, 153.91. Mass spec. calc. for  $\text{C}_{16}\text{H}_{10}\text{OS}_3$ : 314, found 249 ( $\text{C}_{12}\text{H}_9\text{S}_3$ )<sup>+</sup>

## Chapter 4-Computational studies

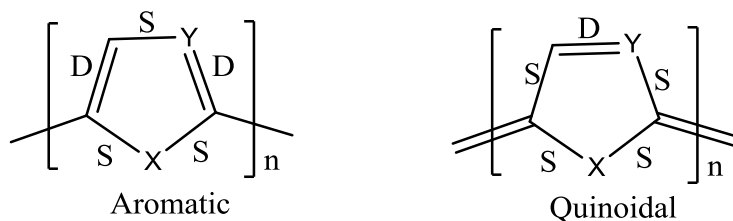
### 4.0 Introduction

As mentioned in chapter 1, much effort has been devoted to the design and synthesis of new organic conjugated materials with low intrinsic band gaps. The smaller this region, the smaller the activation energy required to generate charge carriers. In simple conjugated organic polymers, it can be tuned by modifying the nature of the repeat unit or changing substituents. Among conjugated organic polymers, polythiophene and its derivatives have been most widely studied because of their good environmental stability, useful band gaps ( $\sim 2$  eV), and ease of preparation.<sup>65</sup>

Designing new organic semiconductors is continuing in an effort to improve physical (longevity, processing cost) and material (colour, off-current leakage, and switching speed) characteristics. One key metric is the effective conjugation length within the molecular unit. Lowering the band gap does not improve properties. The band gap must be correctly set for the desired application. It is expected that, for example, a tetramer would have higher conductivity than a trimer.<sup>66</sup>

Bond-length alternation (BLA) is a key physicochemical parameter used in the design of  $\pi$ -conjugated molecular and polymeric materials for a wide range of organic electronic devices.<sup>67</sup> It is a construct that can be used to monitor the amount of polarization in a molecule. The average BLA is defined as the difference between the average lengths of the nominally single bonds (S) and nominally double bonds (D) along a linear  $\pi$ -conjugated backbone. Another metric is the formal binding character of the monomers, the two extremes being the aromatic and the quinoidal forms as shown in Scheme 4.1

### Scheme 4.1: Aromatic vs quinoidal character



Where X = S, Se, O, NH and Y = CH or N

By this definition, an aromatic compound (Ar) with D less than S will have BLA less than zero. Conversely, a quinoidal compound (Q) with D greater than S leads to a BLA greater than zero. For perfect delocalization, where D equals S, the BLA is zero. This can only occur when the symmetry of the molecule allows it, *e.g.* C<sub>6</sub>H<sub>6</sub> in D<sub>6h</sub> symmetry. This will not be the case for heteroaromatic rings of lower symmetry that have unequal distribution of  $\pi$ -electrons due to the differing electronegativities.

The localization index (LI), as defined in the quantum theory of atoms in molecules, is a convenient tool for the analysis of molecular electronic structure from an electron-pair perspective.<sup>68, 69</sup> The electron localization index of an atom is the average number of electrons localized on the atom. Since electrons are either localized within the *ith* atomic basin or delocalized between that basin and every other basin in the molecule, the LI of that atom plus half of the sum of all delocalizing index (DI) for this atom (totaling  $n - 1$ , where  $n$  is the number of atoms in the molecule) yields the total electron population of that atom. Therefore, the total number of electrons in the molecule can hence be expressed as the sum of two separate populations: a localized electron population and a delocalized electron population.<sup>70</sup> The delocalization index is defined as the average number of electrons in an atom that are shared between one atom and other atoms of a molecule. In an effort to see if the addition of new units

into a conjugated system will decrease the electron localization (increase the delocalization) and therefore decrease the band gap, we seek to employ the localization index to determine the amount of localization in monomers and compare them to the amount of localization in oligomers. It is expected that increasing the number of units or conjugation length will result in less localization.

As mentioned in the introduction, the overarching goal of this thesis is to investigate the opto-electronic effect of introducing electron withdrawing heterocycles (thiazole, pyrrole, furan, or selenophene, which has a smaller electronegativity than thiophene) into an oligomeric system. The nature of the heteroatom in the ring will affect the electronic properties of that ring and its ability to conjugate with its neighbour(s), therefore tuning (changing) the HOMO and LUMO energies. This in turn would affect properties such as colour (LEDs), photon absorption profile (photovoltaics), or conduction type (*p* or *n*-type activity in a transistor).<sup>32</sup>

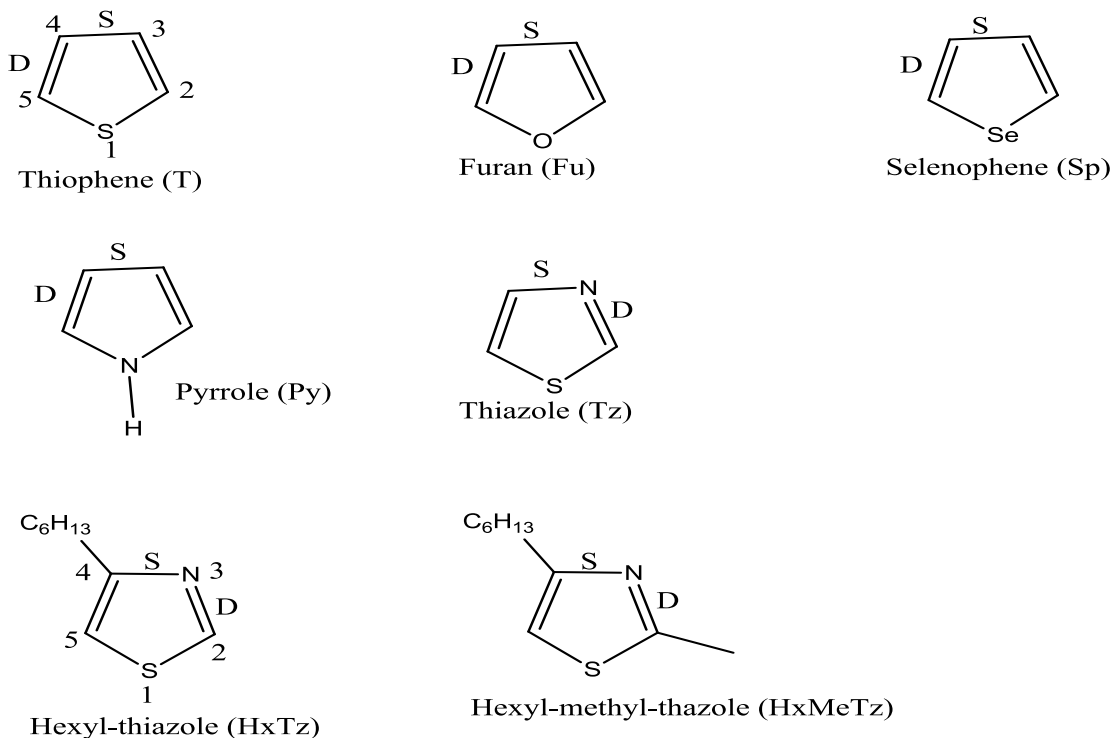
In order to investigate a wider array of possibilities than would be synthetically feasible, we performed a computational study using Gaussian *16* software.<sup>71</sup> Geometry-optimization and frequency assessments were performed via density functional theory (DFT) using the  $\omega$ B97XD/Def2TZVPP model chemistry, which was chosen based on some recent publications as being the best to use for the purpose of this study.<sup>72, 73, 74</sup> In this chapter, we present the HOMO and LUMO energies and the resulting band gaps derived from them and measure the degree of localization/delocalization and inter-ring conjugation. The HOMO and LUMO energies were derived from the formatted checkpoint files in Gaussian and the difference between them gave the band gap of the resulting compound.<sup>75</sup> The localization index corresponds to the number of electrons localized in an atom and the delocalization index is the number of electrons delocalized between two atoms. They are interchangeable measurements because the sum of the two values

must sum to the total number of electrons. Localization indices were obtained using AIMALL, a program based on quantum theory of atoms in molecules, QTAIM.<sup>76</sup> The bonds used for BLA analysis are labelled (S and D) in Scheme 4.1. The dimers and tetramers were chosen as tenable synthetic targets (in some cases lacking probable pendant alkyl groups). Due to the size of the calculation, a more limited selection of tetramers were studied as models for estimating solid-state band gaps.

## 4.1 Monomers

$\omega$ B97XD/Def2TZVPP optimization-frequency computational results for the monomers are summarized in Table 4.1, which includes the HOMO-LUMO energy, BLA, and the localization index. Below in Scheme 4.2 are the monomers used in this study to determine if the monomer will be more aromatic or quinoidal.

**Scheme 4.2: Monomers**



### 4.1.1 HOMO-LUMO energies/band gaps

We consider thiophene to be our “base unit” heterocycle, since it is the most common heteroaromatic system used in molecular electronics. When changing from T to Sp to Fu to Py, the HOMO energies move up (become less negative) in energy from -8.70 for T to -7.93 for Py. On the other hand, the unsubstituted thiazole ring Tz has a lower (more negative) HOMO. As expected, the addition of donating alkyl groups causes the energy to creep back up, and in fact HxTz and T have essentially the same HOMO energy (and disubstituted HxMeTz is higher).

The LUMO energies do not follow the same order as the HOMO energies. The most significant drop in energy was seen in the thiazole (0.97 eV) compared to the thiophene (1.39 eV) as expected because of the introduction of an electron withdrawing group.<sup>5,38</sup> HxTz (1.20 eV) and HxMeTz (1.30 eV) LUMO energies were lowered compared to thiophene. Selenophene’s LUMO (1.17 eV) is also lowered compared to thiophene. The rest of the monomers had LUMO energy greater than thiophene's.

Because the HOMOs and LUMOs do not change in the same order, the resulting band gaps do not follow a neat trend either as seen in Table 4.1. As explained above, we will use the terms “HOMO-LUMO gap” and “band gap” interchangeably, even if the latter specifically refers to a solid-state property, because the width of the bands in organic molecules is very small. Py and Fu have larger band gaps than T (by 0.69 eV and 0.53 eV, respectively), while Sp’s is the smallest (0.27 eV smaller than T), suggesting that the heteroatom’s row number is the determining factor. Further evidence comes from the fact that T and Tz have essentially the same band gap, since the difference between the two is the substitution of CH by N. Introduction of substituent group(s) on the thiazole decreases the band gap as well, shrinking it by approximately 0.17 eV for each alkyl added. This was also noted by Stearman *et al.* they concluded that

substituents introduced into the ring of  $\pi$ -conjugated systems decreases the band gap by influencing the availability of nonbonding electrons that affect the probability of a  $\pi^*$  transition.<sup>77</sup>

### 4.1.2 Bond length alternation

The monomer BLA calculation will define our aromatic bond lengths for each ring type. Scheme 4.2 shows the different monomers and their corresponding nominal double bond and single bonds used in the determination of the BLA; as mentioned above, D is not equal to S in 5-membered heteroaromatic rings. Table 4.1 gives the bond length alternation of the various monomers used in this study. Thiazole's BLA moved up (increased or less negative) with the addition of a substituent (hexyl group). Of the monomers we investigated, one single-ring series exists, which is the Tz, HxTz, HxMeTz series, going from having no alkyl substituents to one to two. The BLA of unsubstituted Tz is  $-0.072 \text{ \AA}$ . Curiously, HxTz (one substituent) has a smaller alternation while the HxMeTz has a larger alternation, suggesting that the former is more quinoidal while the latter is less quinoidal than the base Tz ring.

### 4.1.3 Localization index

These monomer localization index values are simply the base values that we will use for each ring in order to determine the electronic effect when we then move to multi-ring oligomers. As a means of assessing the amount of delocalization, we present the total number of electrons localized within the ring, which is the number of electrons not delocalized. The data presented in Table 4.1 gives the LI for each aromatic ring system, normalized to the number of valence electrons for ease of comparison (i.e., the core electrons have been subtracted off, two for each 2nd-row element, ten for each 3rd-row element, and twenty eight for each 4th-row element). It would appear from this limited data set that substituent groups affect the LI very little – there is a

far greater difference upon changing the heteroatom than there is when adding a hexyl (comparing entry 5 to entry 6 and 7 in Table 4.1).

**Table 4.1:  $\omega$ B97XD/Def2TZVPP HOMO-LUMO energy/band gap, BLA, and effective localization index of the monomers**

Entry #	Monomer	HOMO (eV)	LUMO (eV)	Band gap (eV)	D (Å)	S (Å)	BLA (Å)	Effective LI
1	T	-8.70 <sup>a</sup>	1.39	10.09	1.361	1.420	-0.059	12.37
2	Fu	-8.50	2.12	10.62	1.351	1.430	-0.079	13.14
3	Sp	-8.65	1.17	9.82	1.354	1.430	-0.076	12.42
4	Py	-7.93	2.85	10.78	1.369	1.419	-0.050	11.81
5	Tz	-9.17	0.97	10.14	1.295	1.367	-0.072	14.09
6	HxTz	-8.73	1.20	9.93	1.297	1.367	-0.070	14.08
7	HxMeTz	-8.44	1.30	9.74	1.294	1.369	-0.075	14.05

<sup>a</sup> Experimental value for the HOMO energy of thiophene is - 8.89 eV <sup>78</sup>

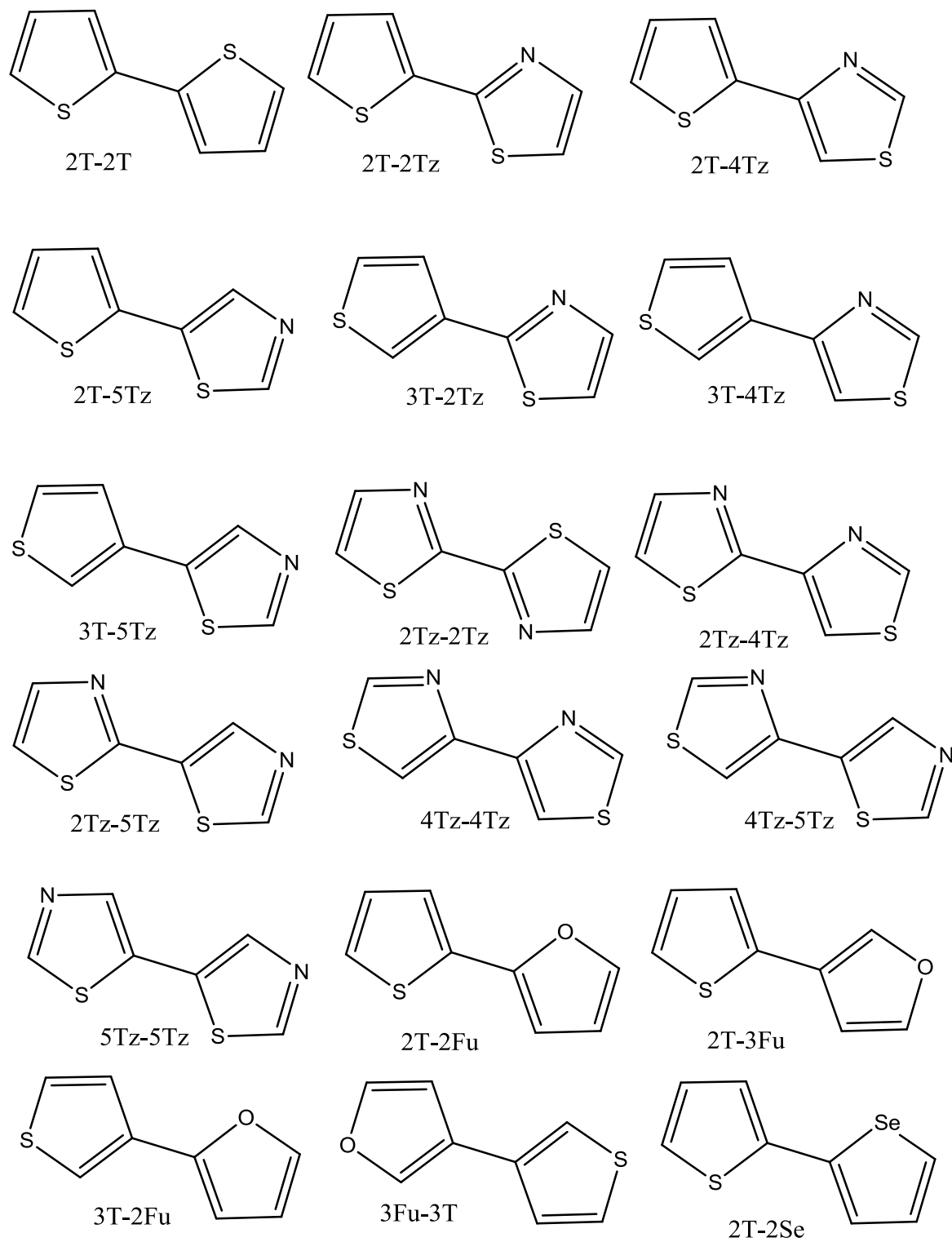
## 4.2 Dimers

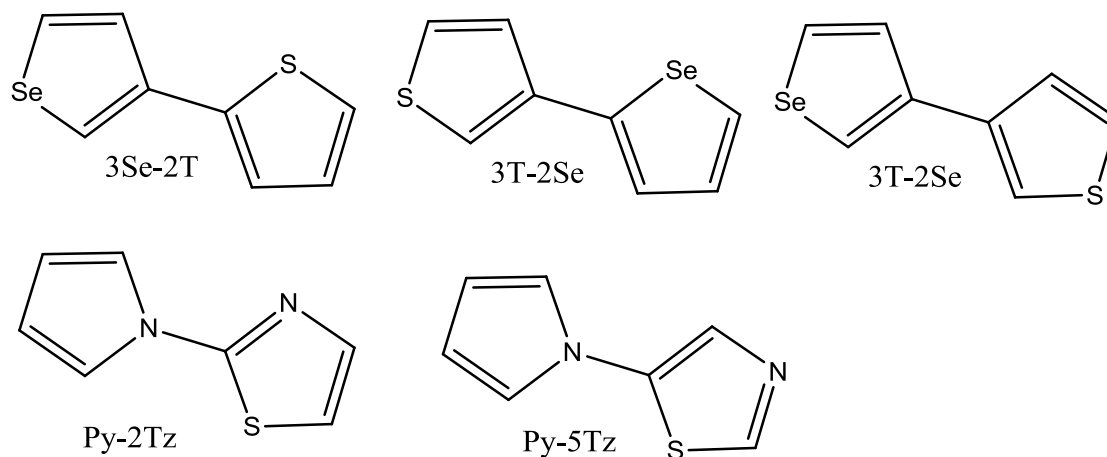
In this section, we explore the effect of replacing thiophene with another heterocycle in an oligomeric molecule. We want to see the differences between bithiophene (T2) and dimers containing one T and one other heterocyclic ring. The differences we are interested in are HOMO and LUMO energies, band gap (estimated from the difference between HOMO and LUMO), and inter-ring electronic communication. The latter is measured by the BLA (the less negative (more quinoidal), the more interaction) and the localization index (LI should decrease



as electron density is shared over multiple rings). This also results in a smaller band gap and shortening of the inter-ring C-C bond. Both the nature of the ring and the location of attachment (regioisomer) will be compared. 2,2'-Bithiophene, (2T-2T) will be considered the base unit of comparison because that is by far the most common bithiophene linkage in thiophene-based functional materials. The dimers used in this study are shown below in Scheme 4.3.

## Scheme 4.3: Dimers





#### 4.2.1 HOMO-LUMO energies/band gap

Upon formation of dimers, HOMO energies will tend to rise, LUMO energies fall, and therefore the band gap shrink. This is exemplified in 2T-2T, where the HOMO energy increases from -8.70 eV for T to -7.67 eV for the dimer. Similarly, the LUMO changes from 1.39 eV to 0.31 eV, and the band gap decreases from 10.09 eV to 7.98 eV.

Moving to thiophene-furan dimers, there are four regioisomers to be considered, because each ring can be substituted at the 2- or 3-position. It is seen in Table 4.2 that all HOMO energies move up considerably with respect to the monomers (-8.70 eV for thiophene, -8.50 eV for furan). The isomers containing a 2-furan have HOMO energies of -7.57 eV (2T-2Fu) and -7.65 eV (3T-2Fu), both of which are lower than 2T-2T (-7.67 eV); the other two regioisomers have higher-energy HOMOs. The LUMO energies for all thiophene-furan dimers are considerably larger than for 2T-2T. The lowest LUMO energy is seen in 2T-2Fu (0.58 eV) as well, lower than the LUMO energies of the respective monomers (1.39 eV for thiophene, 2.12 eV for furan), but higher in 2T-2T (0.31 eV). As a result, the lowest band gap, found in 2Fu-2T, is a bit higher than in 2T-2T. Therefore, we found that the 2-2 linkage has a significantly smaller

band gap than any of the other isomers primarily due to the large decrease in the LUMO. The 3-linkage on either ring increases the band gap but the effect is greater on the Fu than the T.

Turning to the thiophene-selenophene dimers, we again find that the lowest HOMO energy is found in the 2-2 isomer, which is lower than 2T-2T (7.98 eV), and generally, the T-Sp dimers mimic the results of the T-Fu dimers: attachment at the third-position increases the band gap. The only significant difference is that the dimer 2T-2Sp (7.84 eV) has a slightly smaller band gap than 2T-2T.

There are three possible sites of attachment on the lower-symmetry thiazole rings, the 2-, 4-, and 5- positions (S is position 1, N is position 3), giving a total of six thiophene-thiazole dimers. Again, 2T-2Tz (-8.00 eV entry number 10), has the lowest HOMO energy, lower than what was found in 2T-2T (-7.67 eV). The LUMO is also lowered significantly, from 0.31 to 0.05 eV. The 2Tz and 5Tz attachments are virtually identical when attached to the 2T position but this is not the case when attached through the 3T position. The 3T attachment continues to follow the trend noted above, i.e. the HOMO and LUMO are both higher in energy and the band gap is larger relative to the 2T counterpart; this is also true for the 4Tz attachment, which always has a higher energy HOMO and LUMO and the largest band gap when compared to the equivalent 2Tz and 5Tz isomers. Replacing the thiophene with a thiazole lowers the HOMO energies, which is what is expected due to replacement of CH with a more electronegative N. The lowest band gap was observed in 2T-2Tz (8.05 eV), which is comparable to the band gap observed in 2T-2T (7.98 eV) as seen in Table 4.2.

Considering the Tz-Tz dimers of which there are six regioisomers, there are no obvious systematic trends. Naturally, the HOMO energies of all the thiazole-thiazole isomers moved up

in comparing to the monomer (-9.17 eV). The lowest of which was found in entry number 19, 4Tz-4Tz (-8.20 eV), which was a bit higher than what was observed for the HOMO of 2T-2T (-7.67 eV). The LUMO energies dropped considerably in comparison with the LUMO energy of thiazole monomer (0.97 eV), the lowest being 5Tz-5Tz (-0.17 eV). The thiazole monomer has a band gap of 10.14 eV while the thiazole-thiazole dimers range from 8.11 (2Tz-2Tz) to 8.91 (4Tz-4Tz) eV, as compared to the 2T-2T dimer at 7.98 eV (See Table 4.2 below). The 4Tz attachment leads to the largest band gap.

Since only Py-Tz isomers are synthetically accessible at this time, it is the only dimer to feature the Py ring (attached through the N of the pyrrole). Of this very limited set, the two isomers show little difference in HOMO (-8.24 eV for Py-2Tz and -8.20 eV for Py-5Tz) and LUMO energies (0.59 eV for Py-2Tz and 0.53 eV for Py-5Tz), and therefore very similar band gaps of 8.83 and 8.74 eV respectively.

In all the dimers, replacing the thiophene rings with an electron withdrawing group helps lower the HOMO energies and increase the band gap. The only dimer with a lower band gap than 2T-2T (7.98 eV) was that of 2T-2Sp, which had the lowest band gap observed at 7.84 eV.

**Table 4.2:  $\omega$ B97XD/Def2TZVPP HOMO-LUMO energy/band gap of the dimers**

Entry #	Dimer	HOMO (eV)	LUMO (eV)	Band gap (eV)
1	2T-2T	-7.67	0.31	7.98 <sup>a</sup>
2	2T-2Fu	-7.57	0.58	8.15
3	2T-3Fu	-7.81	0.80	8.61
4	3T-2Fu	-7.65	0.89	8.54
5	3T-3Fu	-7.86	0.86	8.72

6	2T-2Sp	-7.66	0.19	7.84
7	3T-2Sp	-7.77	0.44	8.21
8	3T-3Sp	-7.82	0.85	8.67
9	2T-3Sp	-7.71	0.47	8.19
10	2T-2Tz	-8.00	0.05	8.05
11	2T-4Tz	-7.89	0.46	8.35
12	2T-5Tz	-8.02	0.07	8.09 <sup>b</sup>
13	3T-2Tz	-8.11	0.34	8.45
14	3T-4Tz	-8.03	0.78	8.81
15	3T-5Tz	-8.26	0.48	8.74
16	2Tz-2Tz	-8.33	-0.22	8.11
17	2Tz-4Tz	-8.26	0.22	8.48
18	2Tz-5Tz	-8.38	-0.19	8.19
19	4Tz-4Tz	-8.20	0.71	8.91
20	4Tz-5Tz	-8.28	0.23	8.51
21	5Tz-5Tz	-8.40	-0.17	8.24
22	Py-2Tz	-8.24	0.59	8.83 <sup>b</sup>
23	Py-5Tz	-8.20	0.53	8.74

<sup>a</sup> Experimental HOMO-LUMO gap for solid 2T-2T is 4.0 eV for 2T-2T based on electron-energy loss spectroscopy (EESL)<sup>79</sup>

<sup>b</sup> Calculated values at the B3LYP/6-311G(d) level of theory have been reported as 4.7 eV for 2T-5Tz and 4.8 eV for 2Py-5Tz (not *N*-substituted, which is the compound we are reporting)<sup>80</sup>

#### 4.2.2 Delocalization

Three measures were used to study the amount of delocalization (inter-ring electronic communication): the inter-ring C-C bond distance, intra-ring BLA, and LI. When comparing the

inter-ring bonds, we will use 2T-2T as a base number and assume that the rings all have similar sterics (this is a good assumption because in all the dimers, the *anti* configuration was used). For the base level of electron localization and bond-lengths, we will use the values for each monomer and compare to the values in the dimer. In the quinoidal form, **Q**, the S-bond becomes shorter while the D bond becomes longer, therefore, the BLA = D – S will become *less negative* as you move from **AR** to **Q** as seen in Scheme 4.2 above. Localization index should *decrease* in each ring due to inter-ring delocalization. All of these three measures should give congruent results.

To check the conjugation between the rings, we looked at the C-C bridge of the various dimers to see which one gave the shortest bond. The shorter the bond, the higher the inter-ring conjugation and the more quinoidal the bond and the more electron delocalization within the rings. The sum of the electron localization index of the various dimers used in this study are reported in Table 4.3. Again, we will use the respective monomers as our comparison points for BLA and LI. For inter-ring bond distance, we will compare with that of 2T-2T, which has a C-C bond length of 1.454 Å.

Of the four thiophene-furan dimers, 2T-2Fu (entry #2) has the greatest inter-ring communication as evidenced by the three metrics measured here. It has the shortest C-C bond length among its other isomers (1.444 Å) and is even shorter than 2T-2T (entry #1). The other inter-ring bond distances are all significantly longer, but similar to each other, *e.g.* 3T-2Fu (entry #4) and 3T-3Fu (entry #5) are virtually identical, 0.060 Å longer than the shortest example. Turning to the bond-length alternation (BLA) values, it appears that the position of substitution does have a significant effect. The thiophene ring in the three 2T dimers (2T-2T, 2T-2Fu, and 2T-3Fu) have virtually identical BLAs (within 0.03 Å of each other), while the 3T dimers have significantly larger (more negative) BLAs (0.059 Å and 0.060 Å), indicating less quinoidal

character for that ring. Interestingly, the substitution location of the neighbouring furan ring does not have an effect on the BLA of the thiophene ring.

The evidence from the BLA and inter-ring C-C bond length both suggest that the 2-isomers are more quinoidal than 3-isomers, suggesting greater inter-ring delocalization. The localization index, although giving numerically (and percentage-wise) smaller differences, shows the same trend. The 2T-2T dimer has a thiophene ring localization value of 14.25 while both the 2T-furan isomers are 14.26 (slightly more localized). However, the 3T-furan dimers show a larger LI at 14.28. The same trend is seen for the furan ring, where the LI is larger for the 3T isomers than for the 2T isomers. Curiously, as noted for the BLA, the regioisomerism of the thiophene ring is more important than that for the furan ring, even for the furan's parameters.

The inter-ring bond lengths in the thiophene-selenophene dimers behave in perhaps the most systematic way of all those investigated. The bond length of the 2T-2Sp (entry #6) is shortest (shorter than 2T-2T by 0.002 Å). The 2T-3Sp (entry #9) and 3T-2Sp (entry #7) are effectively the same and longer, while the 3T-3Sp (entry #8) is longer again, indicating an order for quinoidal contribution (and inter-ring communication) decreasing through the order 2-2 > 2-3 = 3-2 > 3-3 as seen in Table 4.3 below.

Unfortunately, the BLA and LI metrics are not quite so straightforward. The BLA agrees that 2T-2Sp is the most quinoidal with the smallest BLAs (-0.047 Å and -0.061 Å for the T and Sp, respectively). However, the BLA for all four isomers shows that each ring's regiochemistry is the sole arbiter of its BLA in the resulting dimer: the 2T isomers have BLAs very close to each other (-0.047 Å and -0.050 Å), while the 3T isomers both have BLA of -0.060 Å for the T ring. Similarly, the 2Sp isomers are close (-0.061 Å, -0.063 Å), both of which are considerably smaller than the 3Sp isomers (-0.074 Å) when considering just the Sp ring. Considering the LI, the



dimers in both rings were all localized compared to their respective monomers (12.42). This is, in fact, true of all the rings, the LI is larger for every ring system in the dimer as compared to the monomer. Considering the thiophene ring, 2T-2Sp (12.20) had the most localization of electrons followed by 3T-3Sp (12.28). The electrons of the 2T-2Sp are even more localized than what was observed in both rings of 2T-2T dimer (12.25). In the selenophene ring, the most localized was seen in the 2T-2Sp (entry #6) and 2T-3Sp (12.30) followed by 3T-2Sp and 3T-3Sp dimers (12.32). The selenophenes are insensitive to substitution position – all the LI's are very close for the four dimers studied. All three metrics give congruent results.

In the thiophene-thiazole dimer, 2T-2Tz(entry #10) had the shortest C-C bond length (1.451 Å), shorter than what was observed in 2T-2T (entry #1) (1.454 Å). The other isomers had a bond length greater than observed in 2T-2T, with 2T isomers shorter than 3T and thiazoles in the order 2Tz < 5Tz < 4Tz. The BLA data show the same results. On the thiophene ring, the 2T BLAs are very similar and significantly smaller (more quinoidal) than the 3T dimers. Likewise the thiazole values order 2Tz < 5Tz < 4Tz for both pairings (with 2T and with 3T). Interestingly, the differences on changing regioisomers are very close to 0.010 Å in every case. Concluding, the 2-position gives the most quinoidal ring, the 4 position the most aromatic, and the 5-position is in between. Unfortunately, the LI results are not as cohesive. While 2T-2Tz has the smallest combined LI, and 2T has (mostly) smaller LI than 3T, the largest combined LI (least delocalized) is not the expected 3T-4Tz (entry #14). In fact, a close inspection of the LI data for the Tz ring show an alarming insensitivity to the regioisomerism of the ring, and even when there is a (slight) difference there is no pattern between the 2T dimers and the 3T dimers (and consequently, no correlation to the BLA ordering). Further, 2Tz is the most localized by the LI metric in both its dimers, the exact opposite of the result from the inter-ring bond distance and

the BLA data. The pyrrole ring in both pyrrole-thiazole dimers has a decrease (less negative) in the BLA (from -0.050 Å to -0.078 Å); however, because the attachment is now through the N (1) position, it implies there is a conjugation effect with the attached thiazole. Interestingly, the regiochemistry of the thiazole ring had no effect on the BLA of the pyrrole, although the LI is slightly smaller. For the thiazole ring in the Py-Tz dimers, both the LI and the BLA suggest greater inter-ring communication when connected through the 5-position than through the 2-position.

**Table 4.3:  $\omega$ B97XD/Def2TZVPP bond length alternation (Å), conjugation between C-C bridge bond distance (Å) and localization index of dimers. All thiophene related dimers are in ring 1 and ring 2 are other rings. In Py-Tz, thiazole is ring 1 and ring 2 is the pyrrole ring. The BLA is defined as the bond length difference between the C4-C5 bond (D) and the C3-C4 bond (S).**

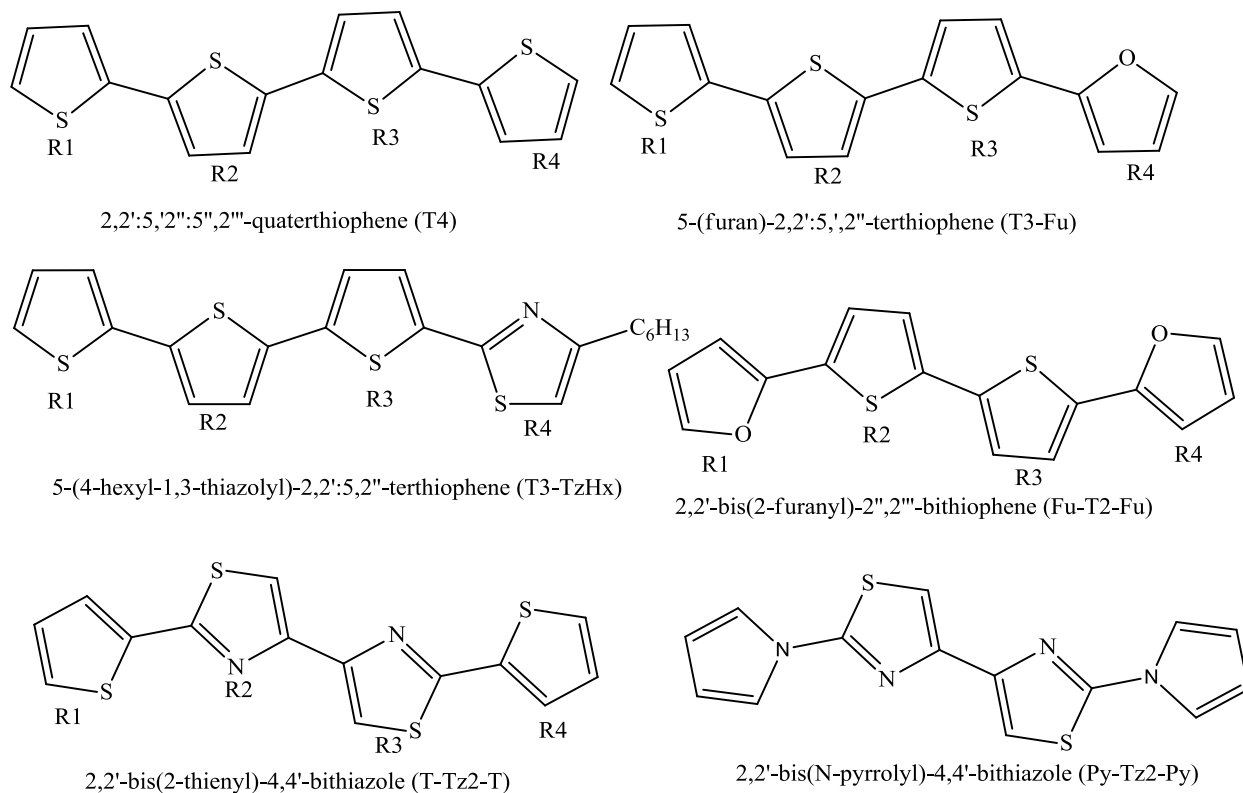
Entry #	Dimers	Ring1				Ring2				C-C bond distance (Å)
		D	S	BLA (Å)	LI	D	S	BLA(Å)	LI	
1	2T-2T	1.368	1.416	-0.048	12.25	1.368	1.416	-0.048	12.25	1.454
2	2T-2Fu	1.367	1.416	-0.049	12.26	1.359	1.426	-0.067	13.01	1.444
3	2T-3Fu	1.366	1.418	-0.051	12.28	1.348	1.437	-0.088	13.01	1.455
4	3T-2Fu	1.367	1.426	-0.060	12.26	1.351	1.426	-0.076	13.05	1.450
5	3T-3Fu	1.359	1.418	-0.059	12.28	1.354	1.430	-0.075	13.06	1.454
6	2T-2Sp	1.368	1.416	-0.047	12.20	1.362	1.423	-0.061	12.30	1.452
7	3T-2Sp	1.368	1.429	-0.061	12.24	1.361	1.42	-0.063	12.32	1.460

8	3T-3Sp	1.368	1.428	-0.060	12.28	1.361	1.435	-0.074	12.32	1.470
9	2T-3Sp	1.367	1.417	-0.050	12.28	1.362	1.436	-0.074	12.30	1.463
10	2T-2Tz	1.368	1.413	-0.045	12.19	1.300	1.363	-0.063	13.99	1.451
11	2T-4Tz	1.367	1.415	-0.048	12.30	1.292	1.373	-0.080	13.96	1.457
12	2T-5Tz	1.368	1.416	-0.048	12.20	1.293	1.364	-0.071	14.42	1.452
13	3T-2Tz	1.367	1.425	-0.060	12.23	1.300	1.363	-0.062	14.02	1.460
14	3T-4Tz	1.366	1.426	-0.060	12.26	1.292	1.374	-0.083	14.00	1.464
15	3T-5Tz	1.368	1.426	-0.058	12.23	1.294	1.364	-0.070	14.00	1.460
16	2Tz-2Tz	1.300	1.362	-0.062	13.92	1.300	1.362	-0.062	13.92	1.454
17	2Tz-4Tz	1.300	1.363	-0.063	13.96	1.293	1.369	-0.077	14.00	1.459
18	2Tz-5Tz	1.300	1.363	-0.063	13.92	1.297	1.362	-0.064	13.97	1.451
19	4Tz-4Tz	1.292	1.372	-0.079	14.00	1.292	1.372	-0.079	14.00	1.462
20	4Tz-5Tz	1.293	1.372	-0.079	13.94	1.297	1.363	-0.065	13.94	1.456
21	5Tz-5Tz	1.293	1.363	-0.070	13.97	1.293	1.363	-0.070	13.97	1.450
21	Py-2Tz	1.291	1.369	-0.078	11.71	1.361	1.425	-0.064	13.69	1.386
23	Py-5Tz	1.289	1.367	-0.078	11.68	1.363	1.421	-0.057	13.65	1.392

## 4.3 Tetramers.

Due to the computational complexity of the increased molecular size, only a few tetramers were studied, because they are synthetically and computationally feasible *i.e.* the six compounds shown in Scheme 4.4.

**Scheme 4.4: Tetramers**



### 4.3.1 HOMO-LUMO Energies/ band gap.

Once again, we will be reporting energy differences between the highest-occupied molecular orbital (HOMO) and the lowest unoccupied molecular orbital (LUMO), using the terms “HOMO-LUMO gap” and “band gap” interchangeably. As expected, there is a decrease in band gap as conjugation length increases. This result is true for all the tetramers relative to any of the dimers, which have, in turn, smaller HOMO-LUMO energy gaps than the monomer rings. Several of the tetramers are dimers of the dimers presented in section 4.2, *i.e.* T4, Fu-T2-Fu, T-

Tz2-T, and Py-Tz2-Py. In every tetramer, the tetramer band gaps are smaller than the dimer band gaps as a result of both the HOMO rising in energy (less negative) and the LUMO lowering in energy (less positive, in many cases decreasing into negative numbers).

Once again, in order to compare the effect of switching a thiophene for another heterocyclic ring, we will compare the calculated tetramer HOMO and LUMO energies to that of the “base form” T4. As expected, each of the electron-withdrawing rings Fu, Tz, and Py caused the HOMO energy to drop stepwise for each substitution. Thus, for the series T4, T3-Fu, and Fu-T2-Fu the HOMO drops from -7.02 eV to -6.99 eV to -6.96 eV. The thiazole drop is even more pronounced. On the other hand, the LUMO energies rise stepwise (*e.g.*, -0.41 eV to -0.35 eV to -0.28 eV for the thiophene-furan series, entry number 1-4). Thus, T4 has the smallest band gap.

**Table 4.4:  $\omega$ B97XD/Def2TZVPP HOMO-LUMO/energy gap (eV) of the tetramers**

Entry #	Tetramer	HOMO (eV)	LUMO (eV)	Band gap (eV)
1	T4	-7.02	-0.41	6.61
2	T3-Fu	-6.99	-0.35	6.64
3	T3-TzHx	-7.19	-0.35	6.84
4	Fu-T2-Fu	-6.96	-0.28	6.68
5	T-Tz2-T	-7.53	-0.09	7.44
6	Py-Tz2-Py	-7.82	0.40	8.22

### 4.3.2 Delocalization

To check the conjugation existing between the rings, we looked at the C-C bridge of the various tetramers to see which of them gave us the shortest bond. The shorter the bond, the higher the conjugation, the more quinoidal the bond and the more electron delocalization within

the inter-rings distances. In the T4 tetramer, the shortest C-C bond is 1.449 Å and comparing with the T-T dimer (1.454 Å) it is seen that there is more conjugation in the tetramer than in the dimer. Our results indicates that the closer the rings are to the middle of an oligomer, the greater the inter-ring conjugation. Our results clearly show this for every measured metric. The inter-ring bond distances decrease from T2 (two exterior rings) to ring 1 – ring 2 in T4 (one exterior, one interior) to ring 2 – ring 3 and T4 (two interior rings), with values of 1.454 Å, 1.451 Å, and 1.449 Å, respectively. The LI similarly drops from 12.25 (exterior rings on both dimer and tetramer) to 12.13 (interior rings in T4) and the BLA suggests the interior rings are more quinoidal (entry #1)

Turning to the rest of the tetramers, the inter-ring bond distances change very little, if they change at all, when moving from the dimers to the tetramers. Thus, the 2T-2Fu linkage changes from 1.444 Å to 1.443 Å on moving from the dimer to the Fu-T2-Fu (ring 1 – ring 2) (entry #4) to the T3-Fu (ring 3 – ring 4) (entry #2). The three T-Tz distances are 1.451 Å and the Tz-Py are 1.386 Å while the Tz-Tz distances are 1.460 Å (entry #5 and 6)

**Table 4.5: ωB97XD/Def2TZVPP C-C bridging and their various bond length (Å) at different position of the tetramers**

Entry #	Tetramer	Ring 1	Ring 2	Ring 2	Ring 3	Ring 3	Ring 4
1	T4	T-T	1.451	T-T	1.449	T-T	1.451
2	T3-Fu	T-T	1.451	T-T	1.449	T-Fu	1.443
3	T3-TzHx	T-T	1.453	T-T	1.451	T-TzHx	1.451
4	Fu-T2-Fu	Fu-T	1.443	T-T	1.449	T-Fu	1.443
5	T-Tz2-T	T-Tz	1.451	Tz-Tz	1.461	Tz-T	1.451

6	Py-Tz2-Py	Py-Tz	1.386	Tz-Tz	1.460	Tz-Py	1.386
---	-----------	-------	-------	-------	-------	-------	-------

**Table 4.6:  $\omega$ B97XD/Def2TZVPP Bond length alternation and localization index of tetramers**

	Ring 1				Ring 2				Ring 3				Ring 4			
	D	S	BLA	LI	D	S	BLA	LI	D	S	BLA	LI	D	S	BLA	LI
T4	1.369	1.416	-0.047	12.25	1.367	1.411	-0.044	12.13	1.367	1.411	-0.044	12.13	1.369	1.416	-0.047	12.25
T3-Fu	1.368	1.416	-0.048	12.25	1.367	1.412	-0.044	12.13	1.366	1.412	-0.046	12.14	1.351	1.425	-0.074	13.02
T3-TzHx	1.368	1.416	-0.048	12.24	1.367	1.412	-0.045	12.13	1.367	1.412	-0.046	12.12	1.296	1.363	-0.067	13.96
Fu-T2-Fu	1.360	1.425	-0.066	13.02	1.368	1.412	-0.044	12.14	1.368	1.412	-0.044	12.14	1.360	1.425	-0.066	13.02
T-Tz2-T	1.367	1.414	-0.046	12.19	1.299	1.367	-0.069	13.89	1.299	1.367	-0.069	13.89	1.367	1.414	-0.046	12.19
Py-Tz2-Py	1.360	1.425	-0.065	11.71	1.289	1.374	-0.085	13.59	1.289	1.374	-0.085	13.59	1.360	1.425	-0.0651	11.71



Turning to the BLA's, we note that in T4 (entry #1), the internal rings (rings 2 and 3) are more quinoidal than the terminal rings (rings 1 and 4). The results continues to be true for all isomers shown in Table 4.6, *i.e.* in those isomers with both an internal and terminal ring of the same type, the BLA is smaller (more quinoidal) for the interior ring. Specifically for thiophene in T3-Fu (entry #2) (-0.048 Å), we note that the terminal ring has a BLA identical to the BLA of 2T-2T (-0.048 Å). Further, as seen for the bond lengths, the BLA for the thiophene rings is smaller than the BLA in the equivalent dimers, which is in turn smaller than the monomer. For example, all the thiophene rings in T3-Fu and Fu-T2-Fu(entry #4) have smaller BLAs (more quinoidal) than 2T-2Fu, which is in turn smaller than the monomer, T. The LI gives the same result (less localization in all tetramer thiophene rings than in any dimer, which in turn is smaller than monomeric T as seen in Table 4.6).

The situation is not as straightforward for the furan ring, which seems to depend on the type of tetramer into which it is inserted, *i.e.* there is a difference between  $C_s$  symmetry of T3-Fu and  $C_{2h}$ -symmetric Fu-T2-Fu, in spite of the fact that the Fu rings are exterior in both cases. The values for 2T-2Fu and the symmetric tetramer are virtually identical for both BLA and LI, whereas the lower-symmetry T3-Fu has larger values, implying less inter-ring delocalization (contradictory to the evidence from the bond distance).

The terminal thiazole in the T3-Tz (entry #2) is attached at the 2-position. Therefore, comparing it to the 2T-2Tz dimer (-0.062 Å), the BLA is larger in the tetramer (-0.067 Å), consistent with what was seen for furan in the asymmetric T3-Fu. The interior thiazole rings are more difficult to directly compare because they are substituted on both the 2 and the 5 positions. Therefore, it is compared with both the 2T-2Tz (which matches the thiophene-thiazole link in the tetramer) and the 4Tz-4Tz dimer (which matches the thiazole-thiazole link). In either case, the LI

values are smaller than either dimer, while the BLA is intermediate between the two.

Interestingly, the interior thiazole rings are almost identical in both LI and BLA for the two tetramers, T-Tz<sub>2</sub>-T and Fu-Tz<sub>2</sub>-Fu, suggesting that the 4Tz-4Tz dimer might be the best model (*i.e.* the 2-substituent has little effect on an interior Tz<sub>2</sub> unit).

Lastly, in the Py-Tz<sub>2</sub>-Py tetramer, we noted that once again, BLA is not a good indicator because of the 1-position substitution, and there is apparently no pattern within the series because the BLA order is monomer < tetramer < dimer. Similarly, looking at the thiazole ring, we note that the pyrrole ring has a much larger effect on the interior thiazoles than either thiophene or furan. Presumably the pyrrole's C-N inter-ring link cannot be treated the same way as an aromatic C-C linkage, even though they are nominally isolobal.

## 4.4 Conclusion

Although there are a couple of minor exceptions (none for the tetramers we investigated), the HOMO drops in energy when a more electronegative ring is substituted for a thiophene. The LUMO energy is far less consistent, leading to variability in the magnitude of the band gap change when substituting rings. The regiochemistry of the inter-ring attachment is also an effective way to tune the band gap. Also, none of the modifications helped decrease the tetramers band gaps beyond that of T<sub>4</sub>, but there was a general decrease in the band gap as conjugation length increase. By extrapolating to a larger number of monomers, the band gap of the polymer can be determined. For example, Zade and Bendikov calculated a T<sub>n</sub> polymer band gap of 2.03 eV using the B3LYP/6-316(d) level of theory.<sup>81</sup> In the dimers, attachment on position-2 seems to be the most favourable in most cases for the thiophene ring compared to position-3. The thiazole values order 2Tz < 5Tz < 4Tz for both pairings (with 2T and with 3T)

4Tz-4Tz dimer might be the best model (*i.e.* the 2 and 5-substituent has little effect on in the thiazole mixed rings system). The three metrics used to measure the inter-ring communication were inter-ring bond length (shorter length = more communication), bond length alternation (as defined here, smaller BLA = more quinoidal = more communication), and localization index (smaller LI = more delocalization = more communication). There were again some minor inconsistencies. Moving from dimers to tetramers does give consistent results, with BLA, and LI both showing that typically rings increase in inter-ring communication when moving from a dimer to a tetramer, with the effect being larger for the interior rings.

## Chapter 5-Conclusion and future work

### 5.1 Conclusion

This thesis covered the synthesis and characterization of compounds containing heterocyclic systems. Toward this end, we successfully synthesized 2-bromo-4-hexyl-1,3-thiazole and 2,2'-dibromo-4,4'-bithiazole as a building block units. These building blocks are synthesized from amino-substituted starting materials, which are inexpensive and readily available. Deamination and conversion to the halo-substituted rings was accomplished using the Sandmeyer reaction. We found the best set of Sandmeyer conditions for thiazoles was copper (II) bromide as the copper halide, *tert*-butyl nitrite as the source of nitrite and distilled acetonitrile as a reaction solvent at 65 °C.

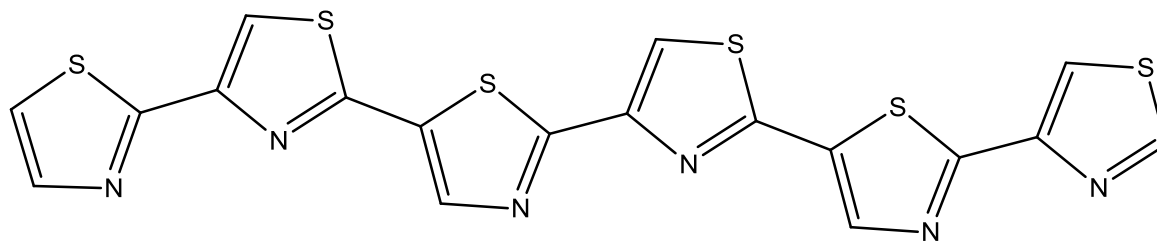
Using these new organic synthons, along with other halogenated, stannylated, or borylated ring systems, we generated several oligomers containing different ring types. In compounds **9**, **11**, **12**, and **14**, we have given evidence that these reaction worked, although further purification and synthetic optimization will be required to make them semiconductor-grade materials. Various coupling methods were employed as compound **9** and **11** were synthesized using the Kumada coupling reaction employing  $(\text{Ni}(\text{dppp})\text{Cl}_2)$  as the catalyst, **14** was synthesized by the Suzuki reaction, and **12** was synthesized by the Clauson-Kaas pyrrole synthesis.

In computational studies, the properties of a number of uncommon heterocyclic rings (uncommon for molecular semiconductors) were tested against oligothiophene base systems to determine the effect of the different rings. As expected, the more electron-donating selenophene increased the HOMO energy. The other, electron-withdrawing rings lowered the HOMO, again

as expected, with the exception of furan, which raised the HOMO instead. Increasing the conjugation length decreases the band gap of the various compounds. Three indices were probed to determine the degree of inter-ring electronic communication: C-C bond length in the linking C-C bond, bond length alternation (BLA) of the bonds within the ring, and localization indices for the rings. Generally, all these measures gave the same information. There is a significant effect on the inter-ring communication depending on the substitutional position of the ring. Generally, chalcogenophene rings attached at the 3-position are less conjugated with their neighbouring ring(s) than those attached at the 2-position. Similarly, the 2- and 5-positions of the thiazole are more conjugating than the 4-position. The attachment positions also had an effect on the HOMO and LUMO energies of the oligomers (and therefore the band gaps).

## 5.2 Future work

Work on these materials will continue, specifically, in attempting to further purify them in order to measure their optoelectronic properties (absorption and emission spectra, both solution and solid state) and semiconducting properties (mobility, band gap, etc.). Another interesting target will be selenophene-thiophene dimers, which give rise to dimers with smaller band gap, even much lower than what was observed in bithiophene, 2T-2T.<sup>78</sup> Another extension of this work aims to develop synthetic methods that will allow us to extend the oligomer size to 6 or more rings. We also would want to work towards all-thiazole oligomers, for example, six thiazole rings with the sulfurs and nitrogens all arranged in the same position to form the following oligothiazole.



Further computational work will also be performed. We plan to compare different functions and basis sets to be sure the trends seen in  $\omega$ B97XD/Def2TZVPP are realistic.

## References

1. Barbarella, G.; Favaretto, L.; Sotgiu, G.; Zambianchi, M.; Bongini, A.; Arbizzani, C.; Mastragostino, M.; Anni, M.; Gigli, G and Cingolani, R., *J. Am. Chem. Soc.*, **122**, 11971 (2000).
2. Liu, Y.; Chen, S.; Cheng, F.; Wang, H. and Peng, Wei. *Sci. Rep.*, **5**, 1-9 (2015).
3. Katz, H. E.; Bao, Z. and Gilat, S. L. *Acc. Chem. Res.*, **34**, 359-369 (2001).
4. Yamashita, Y. *Sci. Technol. Adv. Mater.*, **10**, (2009).
5. Lin, Y.; Fan, H.; Li, Y. and Zhan, X. *Adv.Mater.*, **24**, 3087-3106 (2012).
6. Wu, W.; Liu, Y. and Zhu, D. *Chem. Soc. Rev.* **39**, 1489-1502 (2010).
7. Zahradník, P.; Magdolen, P. and Zahradník, P. *Tetrahedron Lett.*, **51**, 5819-5821 (2010).
8. Getmanenko, Y. A.; Tongwa, P.; Timofeeva, T. V. and Marder, S. R. *Org. Lett.*, **12**, 2136-2139 (2010).
9. Váry, M.; Perný, M.; Kusko, M. and Firický, E., *Elektroenergetika*, **4**, 14-16 (2011).
10. Scharbar, M.C.; Wuhlbacher, D. and Koppe, M. *Adv. Mater.*, **18**, 789-794 (2006).
11. Kumaresan, P.; Vegiraju, S.; Ezhumalai, Y.; Yau, S. H.; Kim, C.; Lee, W. H. and Chen, M. *C. Polym. J.*, **6**, 2645-2669 (2014).
12. Meng, L.; Zhang, Y.; Wan, X.; Li, C.; Zhang, X.; Wang, Y.; Ke, X.; Xiao, Z. and Ding, L. *Science*, **361**, 1094-1098 (2018).
13. Qu, S. and Tian, H. *Chem. Commun.*, **48**, 3039 (2012).
14. Fernandes, S. S. M.; Mesquita, I.; Andrade, L.; Mendes, A.; Justino, L. L. G.; Burrows, H.D. and Raposa, M. M. M. *Org. Electron.*, **49**, 194-205 (2017).

15. Muller, E.; Falcou, A.; Reckefuss, N.; Rojahn, M.; Wiederhirn, V.; Rudati, P.; Frohne, H.; Niyken, O.; Becker, H. and Meerholz, K. *Nature*, **421**, 829 (2002).
16. Gross, M.; Muller, C.D.; Nothofer, H. G.; Scherf, U.; Neher, D; Brauchle, C. and Meerholz K. *Nature*, **405**, 661-665 (2000).
17. Facchetti, A. *Mater. Res.*, **10**, 28-37 (2007).
18. Ying, L. I. U.; Gui, Y. U. and Yunqi, L. I. U. *Sci. China, Ser. B Chem.*, **53**, 779–791 (2010).
19. Sakamoto, Y.; Suzuki, T.; Kobayashi, M.; Gao, Y.; Fukai, Y.; Inoue, Y.; Sato, F. and Tokito, S. *J. Am. Chem. Soc.*, **126**, 8138-8140 (2004).
20. Nyulaszi, L.; Varnai, P. and Veszpremi, T. *J. Mol. Struct. THEOCHEM*, **358**, 55-61 (1995)
21. Ayub, M.; Ayub, K. *J. Chem.*, **2015** 1-12 (2015).
22. Zhang, L; Colella, N. S.; Cherniawski, B. P.; Mannsfeld, S. C. B. and Briseno, A. L. *ACS Appl. Mater. Interfaces.*, **6**, 5327-5343 (2014).
23. Mishra, A.; Ma, C.Q. and Bäuerle, P. *Chem. Rev.* **109** (3), 1141-1276 (2009).
24. Barbarella, G.; Melucci, M. and Sotgiu, G. *Adv. Mater.*, **17**, 1581-1593 (2005).
25. Garnier, F. *Acc. Chem. Res.*, **32**, 209-215 (1999).
26. Garnier, F.; Yasser, A.; Hajlaoui, R.; Horowitz, G.; Deloffre, F.; Servet, B.; Ries, S. and Alnot, P. *J. Am. Chem. Soc.*, **115**, 8716-8721 (1993).
27. Hotta, S.; Waragai, K. *J. Mater. Chem.*, **1**, 835. (1991).
28. Siegrist, T.; Fleming, R. M.; Haddon, R. C.; Laudise, R. A.; Lovinger, A. J.; Katz, H. E.; Bridenbaugh, P.; Davis, D. D. *J. Mater. Res.*, **10**, 2170 (1995).
29. Fichou, D.; Bachet, B.; Demanze, F.; Billy, I.; Horowitz, G.; Garnier, F. *Adv. Mater.*, **8**,



500 (1996).

30. Barclay, T. M.; Cordes, A. W.; MacKinnon, C. D.; Oakley, R. T. and Reed, R. W. *Chem. Mater.*, **9**, 981-990 (1997).

31. MacLean, B. J. and Pickup, P. G. *J. Mater. Chem.*, **11**, 1357-1363 (2001).

32. Facchetti, A.; Deng, Y.; Wang, A.; Koide, Y.; Siringhaus, H.; Marks, T.G. and Friend, R.H. *Angew. Chemie Int. Ed.*, **39**, 4547-4551 (2000).

33. Kunugi, Y.; Takimiya, K.; Yamene, K.; Yamashita, K.; Aso, Y. and Otsubo, T. *Chem. Mater.*, **15**, 6-7 (2003).

34. Jung, E.H.; Seunghwan, B.; Yoo, T. W. and Jo, W. O. *Polym. Chem.*, **45**, 1-7 (2012).

35. Gidron, O.; Diskin-posner, Y. and Bendikov, M. *J. Am. Chem. Soc.*, **132** 2148-2150 (2010).

36. Gidron, O.; Dadvand, A.; Sun, E. H. W.; Chung, I.; Shimon, L. J. W.; Bendikov, M. and Perepichka. *J. Mater. Chem. C.*, **1**, 4358-4367 (2013).

37. Tasch, S.; Brandstätter, C.; Meghdadi, F.; Leising, G.; Froyer, G.; Athouel, L. *Adv. Mater.*, **9**, 33 (1997).

38. Usta, H.; Sheets, W. C.; Denti, M.; Generali, G.; Capelli, R.; Lu, S.; Yu, X.; Muccini, M and Facchetti, A. *Chem. Mater.*, **26**, 6542-6556 (2014).

30. Van Bolhuis, F.; Wynberg, H.; Havinga, E. E.; Meijer, E. W.; Staring, E. G. *J. Synth. Met.*, **30**, 381(1989).

40. Radhakrishnan, R.; Sreejalekshmi, K. G. *J. Org. Chem.*, **83**, 3453 (2018).

41. Goodson, T. I.; Li, W.; Gharavi, A.; Yu, L., *Adv. Mater.*, **9**, 639 (1997).

42. Hoeben, F. J. M.; Jonkheijm, P.; Meijer, E. W. and Schenning, A. P. H. J. *Chem. Rev.*, **105**,

1491–1546 (2005).

43. Hodgson, H. H. *Chem. Rev.*, **40** (2), 251-277 (1947).

44. Lee, J. H.; Curtis, M.D. and Kampf, J.W. *Macromolecules.*, **33**, 2136-2144 (2000).

45. Paula Yurkanis Bruice. *Organic Chemistry*, Fifth Edition, Pearson Prentice Hall, Upper Saddle River, NJ, 2007.

46. Lin, W.; Sun, W.; Yang, J. and Shen, Z. *Mater. Chem. Phys.*, **112**, 617-623 (2008).

47. Liu, Q. X.; Yao, Z. Q.; Zhao, X. J.; Zhao, Z. X. and Wang, X. G., *Organometallics*, **32**, 3493-3501 (2013).

48. Ding, N. W.; Sun, W. L.; Lin, Y. and Shen, Z. Q. *Polym. Sci., (English Ed.* **30**, 759–769 (2012).

49. Cao, J. and Curtis, M. D.. *Synth. Met.*, **148**, 219-226 (2005).

50. Ando, S.; Nishida, J.I.; Inoue, Y.; Tokito, S. and Yamashita, Y. *J. Mater. Chem.*, **14**, 1787-1790 (2004).

51. Bauerle, p; Wurthner, F; Gunther, G. and Effenberger, F. *Synthesis*, **11**, 1099-1103 (1993).

52. Raheem, M. A.; Nagireddy, J. R.; Durham, R. and Tam, W. *Synth. Commun.*, **40**, 2138-2146 (2010).

53. Renaud, P. Lacote E, Quaranta, L. *Tetrahedron Letters*, **39**, 2123-2126 (1998).

54. Josey, A. D.; Jenner, E. L. *J. Org. Chem.*, **27**, 2466 (1962).

55. Kodama, S.; Nakajima, I.; Kumada, M. and Suzuki, K. *Tetrahedron*, **38**, 3347-3354 (1982).

56. Tamao, K.; Sumitani, K.; Kiso, Y.; Zembayashi, M.; Fujioka, A.; Kodama, S.I.; Nakajima, I.;

- Minato, A. and Kumada, M. *Bulletin of the Chemical Society of Japan*, **49**, 1958-1969 (1976).
57. Milstein, D. and Stille, J. K. *J. Am. Chem. Soc.*, **100**, 3636-3638 (1978).
58. Tyrrell, E. and Brookes, P. *Synthesis*, **4**, 469-483 (2004).
- 59 King, A. O.; Okukado, N. and Negishi, E. *J. Chem. Soc. Chem. Commun.*, 683-684 (1977).
60. Bao, Z.; Chan, W. and Yu, L. *Chem. Mater.*, **5**, 2-3 (1993).
61. Grimsdale, A. C.; Chan, K.L.; Martin, R.E.; Jokisz, P.G. and Holmes, A. B., *Chem. Rev.*, **109**, 897-1091 (2009).
62. Irgashev, R. A.; karmatsky, A. A.; Kim, G. A.; Sadovnikov, A. A.; Emets, V.V.; Grinberg, V. A.; Ivanov, V. K.; Kozyukhin, S. A.; Rusinov, G. L. and Charushin, V. N. *Arkivoc J*, **4**, 34-50 (2017).
63. Leermann, T.; Leroux, F. R. and Colobert, F. *Org. Lett.*, **13**, 4479-4481 (2011).
64. Nowakowska-Oeksy, A.; Soloduch, J. and Cabaj, J. *J. Fluoresc.*, **21**, (1), 169-178 (2011).
65. Walsh, A.; Buckeridge, J.; Catlow, C.R.A.; Jackson, A.; Keal, T.W.; Miskufova, M. Sherwood, P; Shevlin, S. A.; Watkins, M. B.; Woodley, S. M.; and Sokol, A. A. *Chem. Mater.*, **25** 2924-2926 (2013).
66. Kwon, O. and McKee, M. L. *J. Phys. Chem., A*, **104**, 7106-7112 (2000).
67. Giesecking, R. L.; Risko, C and Bredas, J-L., *J. Phys. Chem. Lett.*, **6**, (12), 2158-2162 (2015).
68. Bader, R. F. W. *Acc. Chem. Res.*, **18**, 9-15 (1985).
69. Bader, R. F. W. *J. Phys Chem. A.*, **102**, 7314-7323 (1998).
70. Timm, M. J.; Matta, C. F.; Massa, L. and Huang, L., *J. Phys. Chem. A*. **118**, (47), 11304-11316 (2014).

71. Gaussian 16, Revision A.03; M. J. Frisch, G. W. Trucks, H. B. Schlegel, G. E. Scuseria, M. A. Robb, J. R. Cheeseman, G. Scalmani, V. Barone, G. A. Petersson, H. Nakatsuji, X. Li, M. Caricato, A. V. Marenich, J. Bloino, B. G. Janesko, R. Gomperts, B. Mennucci, H. P. Hratchian, J. V. Ortiz, A. F. Izmaylov, J. L. Sonnenberg, D. Williams-Young, F. Ding, F. Lipparini, F. Egidi, J. Goings, B. Peng, A. Petrone, T. Henderson, D. Ranasinghe, V. G. Zakrzewski, J. Gao, N. Rega, G. Zheng, W. Liang, M. Hada, M. Ehara, K. Toyota, R. Fukuda, J. Hasegawa, M. Ishida, T. Nakajima, Y. Honda, O. Kitao, H. Nakai, T. Vreven, K. Throssell, J. A. Montgomery, Jr., J. E. Peralta, F. Ogliaro, M. J. Bearpark, J. J. Heyd, E. N. Brothers, K. N. Kudin, V. N. Staroverov, T. A. Keith, R. Kobayashi, J. Normand, K. Raghavachari, A. P. Rendell, J. C. Burant, S. S. Iyengar, J. Tomasi, M. Cossi, J. M. Millam, M. Klene, C. Adamo, R. Cammi, J. W. Ochterski, R. L. Martin, K. Morokuma, O. Farkas, J. B. Foresman, and D. J. Fox, Gaussian, Inc., Wallingford CT, 2016.
72. Weigend, F. *Phys. Chem. Chem. Phys.*, **8**, 1057-1065 (2006).
73. Head-Gordon, M.; Pople, J.A. *J. Chem. Phys.*, **89**, 5777-5786 (1988).
74. Head-Gordon, M.; Pople, J.A. and Frisch, M. J. *Chem. Phys. Lett.*, **153**, 503-506 (1988).
75. Wong, B. M. and Cordaro, J. G. *J. Phys. Chem. C*, **115** 18333-18341 (2011).
76. Bader, R. F. W. *Chem. Rev.*, **91**, (5), 893-928 (1991).
77. Eakins, G.L.; Alford, J. S.; Tiegs, B. J.; Breyfogle, B. E. and Stearman, C. J., *J. Phys. Org. Chem.*, **24**, 1119-1128 (2011).
78. Refaely-Abramsoh, S.; Baer, R; and Kronik, L. *Phys. Rev. B.*, **84**, 075144 (2011).

79. Steinmuller, D.; Ramsey, M.G.; Netzer, F. P. *Phys. Rev. B.*, **47**, 13323 (1993).
80. Radhakrishnan, R.; Sreejalekshmi, K. G. *J. Org. Chem.*, **83**, 3453-3466 (2018).
81. Zade, S. S.; Bendikov, M. *Org. Lett.*, **8**, 5243-5246 (2006).
82. Heeney, M.; Zhang, W.; Crouch, D. J.; Chabynyc, M. L.; Gordeyev, S.; Hamilton, R.; Higgins, S. J.; McCulloch, I.; Skabara, P. J.; Sparrowe, D. and Tierney, S. *Chem. Commun.*, **47**, 5061-5063 (2007).

## Appendix

The synthesis of several other synthetic (tetrameric) targets were attempted. Intractable products were isolated, consistent with oligomeric compounds of the desired type. Unfortunately, these products were either impure, mixed with other products, or the spectroscopic results were not sufficiently convincing to show a successful synthesis. The experimental details are presented here as a record of the specific routes attempted, out of the many possible synthetic routes to these oligomers.

### Appendix 1.1: Attempted synthesis of 2,2'-bis(2-thienyl)-4,4'-bithiazole (8)

2-Bromothiophene (0.63 g, 3.86 mmol) was mixed with 25 mL of dried ether and added dropwise into magnesium turnings (0.54 g, 22.2 mmol) in 10 mL of dried ether at 0 °C. A pellet of iodine was added at the start to initiate the Grignard reaction. An ice water bath was used to maintain a controlled reflux during the addition process. The resulting mixture was stirred and warmed to room temperature for 3 hours under N<sub>2</sub> (g). A second mixture was prepared containing Ni(dppp)Cl<sub>2</sub> (0.2 g, 0.37 mmol) and 2,2'-dibromo-4,4'-bithiazole (0.42 g, 1.29 mmol) in 30 mL of ether. Both mixtures were cooled to 0 °C. The Grignard reagent solution was cannulated into the catalyst mixture and left to stir overnight under N<sub>2</sub> (g). After this time, the mixture was added to 20 mL of NH<sub>4</sub>Cl, followed by extraction into ether. The organic fractions were dried over MgSO<sub>4</sub>. The ether solvent was removed via rotary evaporation to obtain a yellow solid with a yield of 0.32 g, 65 %. <sup>1</sup>H NMR (500 MHz, CDCl<sub>3</sub>) δ (ppm): 7.09 (dd, 2H, J = 8.1, 5.2 Hz), 7.56 (dd, 2H, J = 5.3, 1.2 Hz), 7.75 (dd, 2H, J = 8.2 Hz), 9.17 (s, 1H). <sup>13</sup>C NMR (126 MHz, CDCl<sub>3</sub>) δ (ppm): 128.74, 131.84, 131.86, 133.28, 135.53, 145.90, 162.40.

### Appendix 1.2: Attempted synthesis of 5,5'-bis (2-(4-hexyl)-thiazolyl)-2,2'-bithiophene (10)

A 2:1 molar ratio of 2-bromo-4-hexyl-1,3-thiazole and 5,5'-dibromo-2,2'-bithiophene was used.

2-Bromo-4-hexyl-1,3-thiazole (1 g, 4 mmol) was weighed into 20 mL of dried ether and the resulting solution added dropwise to magnesium turnings (0.54 g, 22 mmol) in 10 mL of dried ether at 0 °C. A pellet of iodine was added to initiate the Grignard reaction. An ice water bath was used to maintain a controlled reflux during the addition process. The resulting mixture was stirred and warmed to room temperature for 3 hours under nitrogen atmosphere. A second mixture was prepared containing Ni(dppp)Cl<sub>2</sub> (0.1 g, 0.18 mmol) and 5,5'-dibromo-2,2'-bithiophene (0.65 g, 2 mmol) in 20 mL of ether. Both mixtures were cooled to 0 °C. The Grignard reagent solution was cannulated into the catalyst mixture and left to stir overnight under N<sub>2</sub> (g). After this time, the mixture was added to 60 mL of NH<sub>4</sub>Cl, followed by extraction into ether. The organic fractions were dried over MgSO<sub>4</sub>. The ether solvent was removed via rotary evaporation to obtain a yellowish-brown solid. (0.9 g, 67 %). <sup>1</sup>H NMR (500 MHz, CDCl<sub>3</sub>) δ (ppm): 0.88 (t, *J* = 6.6 Hz, 5H), 1.18 – 1.24 (tt, 1H, *J* = 6.5Hz), 1.23 (tt, 3H *J* = 6.5Hz), 1.28 (qt, *J* = 7.2 Hz, 4H), 1.64 (tt, *J* = 15.7, 8.2 Hz, 4H), 2.14 (tt, *J* = 18.6 Hz, 4H), 2.66 (t, *J* = 13.7, 7.6 Hz, 4H), 7.11 – 6.95 (m, 4H), 7.1 (d, *J* = 8), 8.31 (s, 2H), 7.42 (d, *J* = 8.6 Hz, 1H). <sup>13</sup>C NMR (126 MHz, CDCl<sub>3</sub>) δ (ppm): 14.06, 21.34, 26.45, 28.89, 31.19, 31.70, 124.21, 128.88, 131.94, 133.06, 137.85, 143.23, 164.14.

### Appendix 1.3: Attempted synthesis 5-(4-hexyl-1,3-thiazolyl)-2,2':5',2''-terthiophene (13)

2-(Tributyltin)- 2,2':5',2''-terthiophene (2.17 g, 4.04 mmol) and 2-bromo-4-hexyl-1,3-thiazole (1 g, 4.01 mmol) were weighed into a round bottom flask equipped with a stir bar and under

nitrogen gas atmosphere. Tetrakis(triphenylphosphine) palladium(0), (0.23 g, 2.00 mmol) was added to the flask along with 150 mL of toluene, and the solution was refluxed for 3 hours under nitrogen. The resulting mixture was cooled under nitrogen and continued to stir overnight. The solvent was evaporated off with a rotary evaporator. The remaining crude product was dissolved in equal mixture of hexane, ether and ethyl acetate. The product was purified on a silica gel column with equal volume of hexane, ether and ethyl acetate. A yellow powder was obtained (1.32g, 79 %)  $^1\text{H}$  NMR (500 MHz,  $\text{CDCl}_3$ )  $\delta$  (ppm): 0.83 (t, 3H,  $J = 7.0$  Hz), 0.96 – 0.84 (tt, 6H,  $J = 6.45$ ), 1.12 (dd,  $J = 8\text{Hz}$ ), 1.20 (tt,  $J = 6.5\text{Hz}$ ), 1.70 (tt,  $J = 8.0$  Hz, 2H), 2.40 (t, 2H,  $J = 7.20$ ), 7.04 – 6.97 (m, 2H,  $J = 7.20$  Hz), 7.10 (d,  $J = 8.2$  Hz), 7.21 (d,  $J = 8.2$  Hz), 7.22 (dd, 3H,  $J = 8.5\text{Hz}$ ), 7.24 (dd, 1H,  $J = 5.1$  Hz), 7.35 (d, 1H,  $J = 8.3\text{Hz}$ ), 8.35 (s, 1H).  $^{13}\text{C}$  NMR (126 MHz,  $\text{CDCl}_3$ )  $\delta$  (ppm): 28.06, 28.15, 28.24, 28.96, 29.29, 29.69, 125.27, 125.30, 127.65, 127.84, 128.19, 127.40, 128.47, 128.99, 129.27, 133.81, 133.94, 135.20, 136.15, 140.87, 165.70.

#### **Appendix 1.4: Attempted synthesis of 5-(2-furanyl)-2,2':5,2''-terthiophene via Stille coupling (14)**

2-(Tributyltin)-furan (3.27 g, 9.12 mmol) and 5-bromo-2,2':5,2''-terthiophene (3 g, 9.14 mmol) were weighed into a round bottom flask equipped with a stir bar under nitrogen gas atmosphere. Tetrakis (triphenylphosphine)palladium (0) (0.3 g, 0.26 mmol) and 150 mL of toluene were added and the mixture was refluxed for 3 hours. The resulting mixture was cooled under nitrogen and continued to stir overnight. The solvent was removed with a rotary evaporator. The crude product was dissolved in equal parts hexane, ether and ethyl acetate, purified on a silica gel column to give a yellowish-brown powder (2.3 g 70.34 %).  $^1\text{H}$  NMR (500 MHz,  $\text{CDCl}_3$ )  $\delta$  (ppm): 6.51 – 6.43 (d, 1H,  $J = 3, 1.8$  Hz), 6.56 (dd, 1H,  $J = 3.2, 0.8$  Hz), 6.97 (dd, 1H,  $J = 8.5, 4.9$  Hz), 7.09 (d,  $J = 0.5$  Hz, 1H), 7.26 – 7.14 (dd, 2H  $J = 8.6, 1.2$  Hz), 7.33 (dd, 2H,  $J = 8.6$ ), 7.42 (dd, 2H,  $J = 8.8$  Hz), 7.46 (d, 2H,  $J = 8.8$  Hz), 7.72 (d, 1H,  $J = 8.8$  Hz), 7.81 (dd, 1H,  $J =$



1.9, 0.95 Hz).  $^{13}\text{C}$  NMR (126 MHz,  $\text{CDCl}_3$ )  $\delta$  (ppm): 111.23, 123.56, 124.17, 124.35, 127.76, 128.99, 133.23, 136.06, 136.34, 136.99, 137.20, 141.61, 153.90.